Drum centrifuge study of three-leg jackup models on clay

E.T.R.Dean[1], R.G.James[2,3], A.N.Schofield[2,3], and Y.Tsukamoto[4]

Technical Report CUED/D–Soils/TR289
Cambridge University Engineering Department
January 1996

1 Soil Models Limited
2 Cambridge University Engineering Department
3 Andrew N Schofield & Associates Limited
4 Science University of Tokyo

Drum centrifuge study of three-leg jackup models on clay

E.T.R.Dean, R.G.James, A.N.Schofield, and Y.Tsukamoto

Abstract

This paper reports and discusses centrifuge test data of model three-leg jackups on kaolin clay. The tests modelled one prototype jackup with 6.5 metre diameter 13° conical spudcans, one with 6.5 metre diameter flat-based spudcans, and one with 13.0 metre diameter flat-based spudcans.

Keywords: bearing capacity, footing, foundation, plasticity, clay

Contents

1. Introduction

Figure 1 shows features of an independent-leg offshore jackup platform. Typical operations and geotechnical considerations are described by McClelland et al (1982), Young et al (1984), Boswell (1986), Reardon (1986), Poulos (1988), Ahrendsen et al (1989), Chaney and Demars (1991), Senner (1992), Boswell and D'Mello (1993, 1995), SNAME (1994). The unit is typically moved to location with its legs elevated. The legs are then jacked onto the seabed and the jacking systems are used to lift the hull out of the water. Water ballast may be taken on board to preload the foundation. The ballast is then discharged and the hull is raised further to provide adequate air-gap during subsequent operations.

Subsequent environmental loads include wind load (typically 25–35% of the total lateral load), wave (typically 55–65%), and current (10%; Poulos, 1988, p.255). Earthquake effects can be significant in seismic regions, but are not considered here. Control of buoyant weight and of the position of its centroid is important. In this paper, considerations are restricted to loading in the plane of Figure 1. Soil reactions at the i-th spudcan are vertical load Vi, horizontal load Hi, and moment M_i. The moments are important in serviceability and ultimate limit state calculations, and for fatigue, particularly for the spudcan-leg connections and the jacking mechanisms (Santa Maria, 1988; Tan, 1990; Osborne et al, 1991; Murff et al, 1991, 1992).

Much attention has been given to the problem of large spudcan penetration into clays, and to "punchthrough" during landing and preloading, in which failure of a stiff upper crust overlying a weaker stratum leads to rapid penetration of one spudcan (Endley, 1981; Asquer and Antalovsky, 1982; Fujii et al, 1989; Stewart et al, 1989; Hambly 1990). Field data and analyses of jackup performance on clay and clayey-silts were reported by Baglioni et al (1982), McNeilan and Bugno (1985), Arnesen et al (1988), Brekke et al (1989), Hambly et al (1990), Hambly and Nicholson (1991), Stewart et al (1991). Single-gravity test data of spudcans on clay were reported by Santa Maria (1988), Martin (1991), Houlsby and Martin (1992), Martin and Houlsby (1994). Centrifuge data of spudcans on soft clay were reported by Siciliano et al (1989) and Craig and Chua (1991).

This paper describes and discusses data of three centrifuge tests of a model 3–leg jackup on over-consolidated speswhite kaolin clay. Laboratory test data for this clay are reported by Knoyle (1979), Clegg (1981), Airey (1984), Al-Tabbaa (1984, 1987),

Elmes (1986), Al-Tabbaa and Wood (1987), Phillips (1989), Springman (1993). Table 1 lists some of its properties. Table 2 lists details of the three jackup model tests. Moment-fixity aspects of these data were previously reported by Wong et al (1993). This paper focuses on preloading, cyclic loading, and pullout.

2. Experimental apparatus and procedures

2.1 Drum centrifuge

Centrifuge modelling plays a major role in resolving geotechnical issues relating to offshore structures (Rowe et al, 1975, 1976, 1983). Principles and practice of centrifuge modelling for a variety of onshore and offshore geotechnical applications are described by Schofield (1980, 1981), Craig (1983, 1984), Craig et al (1988), Corte (1988), Ko and McLean (1991), Taylor (1994), Leung et al (1994), and others.

Figure 2 shows features of the Cambridge 2-metre geotechnical drum centrifuge configured for jackup and single-spudcan tests on clay. The model container consists of a cylindrical drum 2 metres in diameter and 1 metre high. The inner circumference of $2\pi \approx 6.3$ metres supports a cylindrical ring of sand which is held against the drum wall by the centrifuge "gravity" created by spinning the drum. Two clay samples, prepared as described below and held within steel frames, were placed at opposite positions on the drum wall. Apparatus mounted on the central column was used to carry out single-spudcan and jackup model tests on the clay specimens under elevated centrifuge gravities. Data signals from transducers on the specimens and the testing apparatuses passed through slip rings to automated model control and data acquisition systems in the control room.

In Table 2, the nominal gravity level G_{NOM} is the centrifugal acceleration at the drum wall. Because the centrifuge gravity varies linearly from the soil surface to the drum wall, there is a different gravity level at the inner clay surface, which was at 880mm radius in these tests. For simplicity, the scale factors in Table 2 have been computed from the acceleration $Ng=0.88G_{NOM}$ at the clay surface.

2.2 Clay specimen preparation

The first stage of sample preparation is shown in Figure 3. Speswhite kaolin clay powder was mixed with de-ionised water under a partial vacuum for two hours to

achieve a slurry with a moisture content of 120% by weight. An 850mm diameter steel tub was placed in a consolidometer, a steel plate was placed inside, a porous plastic plate was inserted, and filter papers were placed on it. Clay slurry was transferred into the tub. Filter papers and a porous plastic plate were placed on the clay slurry. The piston was lowered onto the plastic plate. Water pipes were connected to provide drainage through the top and bottom surfaces. Displacement transducers were attached to measure the subsequent vertical compression. Pressure was applied to the back of the piston. Consolidation was carried out in stages, giving total stresses over the 850mm diameter area of the clay of 5, 10, 20, 40, 80, 160, 320, and finally approximately 600 kPa. Sufficient time was allowed at each stage for pore fluid to exit the clay, and for most of the excess pore pressure to dissipate. After sufficient time at the final vertical stress, the loads were reduced at a rate of approximately 120kPa per day. This was judged to be sufficiently slow to avoid cavitation during swelling. At the end of the last stage of unloading, to 100 kPa, the drainage valves at the bottom of the specimen were closed.

Figure 3(b) shows the relation of specific volume V and total vertical stress σ_V during consolidation and unloading. Also shown are one-dimensional consolidation curves obtained in laboratory tests by earlier researchers, plotted in terms of vertical effective stress σ'_V. The horizontal offset between the total stress data and the 1D effective stress consolidation line represents the excess pore pressure at the end of each stage of loading. The final vertical effective stresses at the specimen mid-heights were 594 kPa for the specimen used in test B and 604 kPa for test C.

The next stages of preparation are shown in Figure 4. The vertical stress of 100 kPa at the last step of unloading was released. The piston and plastic plate were removed. The tub was raised. The clay was extruded. A rectangular steel frame with a cutting edge was pressed into the free-standing clay block. Excess clay was then carefully cut away. The frame was rotated, lifted into the drum centrifuge, and placed in position on a 2mm thick layer of geotextile on the drum wall. Partially saturated sand was packed around the frame to hold it firmly in position. A cutting tool was fixed to the central column, and was used to machine the inner surface of the clay to a cylindrical shape. The tool was then removed. Metal pieces were fixed to the frames and displacement transducers were attached. These allowed settlements to be monitored during re-consolidation at elevated centrifuge gravities.

2.3 Jackup and spudcan models

Figure 5 shows details of the model jackup. The vertical downwards direction in this figure corresponds to the radial outwards direction in Figure 2(a). The model consisted of a rigid hull with three tubular legs. A 57.8mm diameter instrumented model spudcan was fitted to the end of each leg. The model was hung from a support frame attached to the central column of the drum centrifuge. Because the total weight W* of the model in the centrifuge gravity was larger than needed, part of the weight was taken by an upthrust U applied to the underside of the hull by the hanger. Thus the sum of the total vertical loads on the three spudcans was W*-U. Horizontal load H_{APP} was applied to the model by cables from actuators on the support frame to the hull reference point "HRP". In end elevation, Figure 2(b), legs numbered 2 and 3 were splayed at ±7°. This meant that the direction along the centreline of these legs corresponded to the local direction of the centrifuge gravity.

In test A, conical model spudcans shown in Figure 6(a) were fitted to the model jackup. In tests B and C, the flat-based spudcans shown in Figure 6(b) were used. The spudcan on the i-th leg housed a loadcell to measure axial load (Pi), shear load (Q_i), and moment (M_i). The axial and shear loads could be resolved to obtain the spudcan vertical loads (Vi) and spudcan horizontal loads (Hi) as follows:

$$V_i = P_i.\cos\theta_i + Q_i.\sin\theta_i - B_i \quad (1)$$

$$H_i = Q_i.\cos\theta_i - P_i.\sin\theta_i \quad (2)$$

where θ_i is the rotation of the i-th spudcan and B_i is the buoyancy upthrust on it. The reason for subtracting B_i is as follows. In the field, Figure 1, the spudcan loads Vi are differences between total loads before and after contact with the seabed. Buoyancy acts both before and after contact, so Vi are equilibrated by the sum of effective stresses at the soil-spudcan interface and excess pore pressure in the soil. In the model test, Figure 5, the fluid surface was at level B, due to apparatus limits. The model spudcans were only partially submerged, and the buoyancy upthrust on them varied with vertical spudcan displacement. The measured loads included buoyancy effects. To obtain the correct relation to a full-size prototype jackup, the buoyancy forces are subtracted in equation 1.

In the following descriptions, vertical and horizontal displacements v_{HULL} and h_{HULL} represent displacements of the hull reference point HRP located as shown in Figure

5. Zeroes for these values are described below. The hull rotation θ_{HULL} is taken as zero when the model jackup is vertical in the centrifuge gravity. The sum of the spudcan vertical loads Vi was taken to be the net buoyant rig weight W. The sum of the spudcan horizontal loads H_i was taken to be the net horizontal load H_{NET}. Spudcan vertical and horizontal displacements (v_i,h_i) and rotations θ_i were inferred by combining the measured hull motions with spudcan motions relative to the hull. These relative motions were calculated from the measured spudcans loads assuming the legs deformed in bending with flexural rigidity EI = 0.234×10^6 kN.mm^2.

2.4 Soil states

At the start of each day of testing, the centrifuge was started and the speed increased to a low speed. Water was then introduced into the partially saturated sand. The phreatic surface moved inwards from the drum wall until the sand and the clay were covered by 1–5 mm of water. The speed was then increased to achieve the desired gravity level for the first test. Settlements of the clay were monitored until primary re-consolidation was complete. The model test was then started.

Dean et al (1992) show that in-situ vertical effective stresses in a drum centrifuge depend slightly on the value of the lateral earth pressure K_o. Consideration of an element of soil between radii r and r+dr from the centrifuge axis, assuming that pore pressures are in equilibrium so that no excess pore pressures occur, gives:

$$\frac{d\sigma'_V}{dr} + \frac{\sigma'_V - \sigma'_\theta}{r} = \rho'.\omega^2.r \qquad (3)$$

where σ'_V is the radial effective stress, σ'_θ is the circumferential effective stress, p' is the buoyant mass density of the soil, and ω is the angular speed of the drum in radians per second. Assuming $K_o = \sigma'_\theta / \sigma'_V$ is constant with model depth $z_M = (r - R_o)$, where R_o is the radius at the inner soil surface, the solution is:

$$\text{For } K_o \neq 3 : \sigma'_V = \rho'.\omega^2.\left\{ r^2 - (R_o^{3-K_o} / r^{1-K_o}) \right\} / (3 - K_o) \qquad (4)$$

$$\text{For } K_o = 3 : \sigma'_V = \rho'.\omega^2.r^2.\ln(r / R_o) \qquad (5)$$

Although this indicates that the relation between effective stress and depth in the model is not linear, the amount of non-linearity is not great. Figure 7(a) shows the

vertical effective stresses for the three tests, each calculated for two values of Ko. Figure 7(b) shows the implied initial vertical over-consolidation ratios, based on the previous maximum effective vertical stresses attained during consolidation in the 850 mm diameter tub.

At the end of each day of testing, the centrifuge was slowed. Water was drained away from the sand to give a partially saturated sand specimen with some effective cohesive strength. The centrifuge was then stopped. Figure 7(c) shows moisture content profiles obtained from samples taken after the centrifuge had been stopped. Figure 7(d) shows undrained strengths obtained from a miniature vane. Based on Almeida (1984) and Springman (1993), actual undrained strengths during the tests at elevated gravities are expected to have been larger than these post-test values.

3. Experimental Results

3.1 Preloading

In the first event of each test, the model jackup was landed onto the soil surface, preloaded vertically, and then partially unloaded.

Figures 8(a–c) show the responses during preloading and unloading. In each diagram, the horizontal axis represents a vertical spudcan load V_{SPUD} divided by the spudcan area $A=\pi B^2/4$ at its widest section. The vertical axis represents spudcan penetration v_{SPUD} divided by spudcan diameter B. In Figures 8(a,b), $v_{SPUD}=0$ represents a best estimate of when the full spudcan diameter penetrated the clay surface. The origins for v_{SPUD} in Figure 8(c) have been adjusted slightly so as to match the response of the spudcan on leg 1, denoted as L1, with those of the spudcans on legs 2 and 3, denoted as L23. The total times from the start of preloading and to the end of unloading are given at model scale (T_M) and prototype scale ($T_P=N^2xT_M$). The prototype times are longer than typical preloading times at field scale. If an appropriate order-of-magnitude estimate for c_V is $0.5mm^2/sec$, based on Al-Tabbaa (1987) and Springman (1993), then the time factor $T=c_Vt/B^2$ is in the range 0.03-0.07 for model loading periods $t=T_M$ of 220–450 seconds. A little drainage of the clay is expected to have occurred during the model preloading, whereas a typical field preloading event on clay would be almost fully undrained.

The data show that large vertical penetrations occurred, and still larger penetrations would have been needed to reach the bearing capacity of the footings. The data of tests B and C include unload-reload excursions prior to reaching the final vertical preload. These excursions show some hysteresis. In Figure 8(d), the vertical axis represents prototype spudcan penetration, equal to N times model penetration. The results for tests B (prototype diameter 6.5 metres) and C (prototype diameter twice as large) are almost identical. At model scale, this indicates that the vertical stress required to achieve a given model penetration was proportional to the rate of increase of vertical stress with model depth. At prototype scale, it indicates the absence of a footing size effect. The vertical stress required to achieve a given prototype penetration was the same for a 13.0 metre diameter spudcan on this clay as for a 6.5 metre diameter spudcan.

3.2 Slow cyclic horizontal loading

After landing and preloading, a sequence of episodes of either rapid or slow cyclic horizontal loading was applied. Table 4 lists the events for each test, together with maximum and minimum values of $H_{NET}/3A$, where $A=\pi B^2/4$ is the cross-sectional area of a spudcan at its largest diameter Cycle times at model scale (T_M) and prototype scale ($T_P=N^2 x T_M$) are also listed. The adjectives “low” and “rapid” here relate to the capabilities of the model actuation system for these tests. Cycle times for the “slow” cyclic loading events were such that some drainage and consolidation is expected to have occurred during cycling. Prototype times for the “rapid” events were also long compared to typical field cyclic periods for an extreme wave.

Figures 9(a–c) shows data of hull responses during “events 3”, in which cycles of horizontal load of increasing amplitude were applied. Two cycles were applied in test A. Three cycles were applied in tests B and C. For each test, the upper diagram shows the average spudcan shear stress $H_{NET}/3A$, where H_{NET} is the sum of the spudcan horizontal loads Hi, plotted versus dimensionless hull horizontal movement $\Delta h_{HULL}/B$, where Δh_{HULL} is the change of hull horizontal position since the start of the event. The lower diagram shows dimensionless hull vertical movements $\Delta v_{HULL}/B$. The data show noticeable hysteresis in the horizontal load-displacement responses, with no clear yield points. The unloading responses are non-linear. Net plastic vertical settlements increase with increasing horizontal load amplitude.

In Figure 9(d), the secant normalised stiffness $(\Delta H_{NET}/3A)/(\Delta h_{HULL}/B)$ is plotted versus normalised horizontal load amplitude $\Delta H_{NET}/3A$, where ΔH_{NET} is the change of H_{NET} from peak positive to peak negative value, and Δh_{HULL} is the change of hull horizontal position from peak positive H_{NET} to peak negative H_{NET}. Comparison of the data of tests A and B indicate that the global response was stiffer for the cones than for the flat spudcans. Comparison of the data for tests B and C for the flat spudcans indicates that, at a given normalised load amplitude $\Delta H_{NET}/3A$, the value of $(\Delta H_{NET}/3A)/(\Delta h_{HULL}/B)$ was smaller in test B, with 6.5 metre diameter prototype spudcans, than in test C, for a prototype rig twice as large with 13.0 metre diameter spudcans.

Figures 10(a–b) show the normalised spudcan loadpaths, plotted in terms of the stress measures Vi/A, Hi/A, and M_i/Z_e, where $A=\pi B^2/4$ is the spudcan area at its widest section and $Z_e=\pi B^3/32$ is the elastic section modulus of the base area. If an applied vertical load V_i and moment M_i are equilibrated by a linear variation of vertical stress across a circular section of diameter B, then the vertical stress at one edge would reach zero if the magnitude of M_i/Ze reached V_i/A. In the upper diagram of each pair, the dotted lines marked "H" indicate the relations $H_i/V_i=\pm 0.5$. A secant moment fixity f_i at the i-th spudcan can be defined as:

$$f_i = \frac{\text{Actual moment at i - th spudcan}}{\text{Theoretical moment for fully encastre spudcan}} = \frac{2\Delta M_i}{\Delta H_i.(L_i + 2S)} \quad \text{.....} \quad (6)$$

where $(\Delta H_i, \Delta M_i)$ are changes of H_i and M_i, L_i is the length from hull-leg connection (HLC) to spudcan-leg connection (SLC), and S is the height of a rigid spudcan from SLC to spudcan load reference point (LRP). If for simplicity it is assumed that the fixities at the spudcans are equal and that the net horizontal load H_{NET} is shared equally by the three spudcans, and if in addition the small differences in leg lengths and in hull-leg connection levels between leg 1 and legs 2 and 3 for the model of Figure 5 are ignored, then consideration of static equilibrium of the model gives:

$$\Delta V_1/\Delta H_1 = 3\{2Y - f.(L+2S)\}/(2D) \quad \text{.....} \quad (7)$$

$$\Delta V_{23}/\Delta H_{23} = -(\Delta V_1/\Delta H_1)/2 \quad \text{.....} \quad (8)$$

where Y is the height from spudcan load reference point (LRP) to hull reference point (HRP), f is the moment fixity, L is the average leg length, D is the leg spacing

in elevation, and suffix 23 denotes leg 2 or leg 3. Taking Y=352mm, L=248mm, S=71.4mm, and D=186mm, this gives $\Delta V_1/\Delta H_1=5.68$ and $\Delta V_{23}/\Delta H_{23}= -2.84$ for pinned conditions (f=0) and $\Delta V_1/\Delta H_1=2.53$ and $\Delta V_{23}/\Delta H_{23}= -1.26$ for encastre conditions (f=1). It is clear from the slopes marked on the diagrams in Figure 10 that the spudcan responses were closer to pinned than encastre.

Figures 11 (a-c) and 12(a–c) show normalised horizontal load-displacement and moment-rotation responses for the spudcans, where $\Delta h_i/B$ is the change of spudcan horizontal position since the start of the event and $\Delta\theta_i$ is the change of spucan rotation. The horizontal load-displacement responses include some signal noise in the $\Delta h_1/B$ values. However, typical shapes of hysteresis loops can be discerned. The data in Figure 11 (b) for test B suggest that a sliding condition was reached at negative H_1 during the second and third cycles. Such a condition can be expected at this spudcan, due to the reduction in vertical load as H_1 increases negatively. However, it is conceivable that an instrumentation limit was reached in these cycles, and that the magnitude of H_1 at which slip occurred was larger than indicated. The moment-rotation data in Figure 12 for the spudcans on legs 2 and 3 also suggest conventional hysteresis loops. However, the moment-rotation data in Figure 11 for the spudcan on leg 1 show more complex shapes.

Figures 13(a–c) show how horizontal loads and moments were shared between spudcans. In each diagram, the horizontal axis represents a quantity for the spudcan on leg 1, the vertical axis represents the corresponding average for the spudcans on legs 2 and 3. The lines E-E mark where the responses would be equal. The data show that larger fractions of the changes of the net horizontal load were taken on the spudcans on legs 2 and 3. The sharing of moments is more complex, but by considering the average slopes from largest negative to largest positive values, it may be concluded that larger cyclic changes of moment occurred at the spudcans on legs 2 and 3 compared to the spudcan on leg 1.

A feature of the data examined above is that moments M_1 at the spudcan on leg 1 were biased negatively, and moments M_{23} at the other two spudcans were biased positively. Figure 14 shows data of event 9 in test C. The hull load-displacement and rotation responses are shown in Figure 14(a). The LVDT displacement transducers measuring horizontal hull displacement malfunctioned at $\Delta h_{HULL}/B \approx 0.055$. The data of hull rotations, which were measured by a separate set of transducers, show that there was continuity of response beyond this value. Figures

14(b1 ,b2) show the moment responses at the spudcans. In each diagram, the vertical axis represents the vertical spudcan load $V_{i,total}$ for the i-th spudcan divided by spudcan area $A=\pi B^2/4$, where $V_{i,total}=V_i+B_i$ includes the buoyancy force Bi. The horizontal axis represents moment, plotted as stress M_i/Z_e. The dotted lines marked T show where the magnitudes of $(V_i+B_i)/A$ and M_i/Z_e are equal. The loadpaths are approximately bounded by the lines $M_1/Z_e = -(V_1+B_1)/A$ for the spudcan on leg 1, and $M_{23}/Z_e = (V_{23}+B_{23})/A$ for the spudcans on legs 2 and 3. The data suggest that the spudcan on leg 1 had become incapable of sustaining significant positive moment, and that the spudcans on legs 2 and 3 had become incapable of sustaining significant negative moment.

A potential starting point towards an explanation for this unexpected moment biasing might be in terms of cyclic opening and closing of a crack down one vertical side of the spudcan, and development of a softened region of soil beneath the spudcan near the crack tip. The crack might limit moments approximately to $|M_i/Z_e|$ less than V_i/A. The softer region might throw the centre of vertical force to the other half of the spudcan bearing area. Further work would be needed to determine whether this or another process caused the development of moment bias.

3.3 Rapid cyclic horizontal loading

Figure 15(a) shows selected time records for one of the rapid loading events in test B. The data are plotted against prototype time Tp, equal to N^2 times model time. The record for the normalised total horizontal load $H_{NET}/3A$ shows an initial period during which the model actuation system was started and the load cycles increased in magnitude, followed by a period of uniform cycling. The data of spudcan settlements show an initial period in which there was upwards movement at the spudcan on leg 1, followed by a period of approximately constant rate of settlement per cycle. Detailed inspection of the data for the spudcans on legs 2 and 3 suggests that there was a slight reduction of settlement rate towards the end of the event.

Figure 15(b) shows relations between the plastic settlement per cycle, plotted as $\Delta v_{SPUD}/B$ on the vertical axes, versus cyclic amplitude of spudcan vertical load, plotted as $\Delta V_{SPUD}/A$, where ΔV_{SPUD} represents the change in vertical load on a spudcan between the times of peak positive and peak negative net horizontal load H_{NET} in a cycle. The data include all the rapid cyclic loading tests listed in Table 4, and are for the periods of uniform cycling in these events, excluding the start-up

period of the model cyclic loading actuation system. The data for tests A and C indicate that there are threshold values of cyclic vertical spudcan load amplitude below which negligible plastic settlements occur. The threshold values of $\Delta V_{SPUD}/A$ were about 20kPa in test A and about 46kPa in test C. The existence of a threshold is consistent in general terms with the idea of a spudcan yield locus, described for clays by Santa Maria (1988) and Houlsby and Martin (1992). Continuing settlements in uniform load cycles indicates the settlements may be due to sub-yield plasticity.

In Figure 16(a), the hull horizontal load-displacement data for three events in test A are shown. The data are for negatively biased cyclic loading in event 4, two-way loading in event 2, and positively biased loading in event 6. In all three events there is hysteresis in individual cycles. The drifts show there was a steady accumulation of hull horizontal displacements for two-way cycling and positively-biased cycling. Figure 16(b) shows spudcan settlements during these events. All six diagrams are to the same scales. There were very small settlements in one-way cycling. There were large cyclic settlements in the two-way cycling, with the spudcan on leg 1 settling more than the spudcans on legs 2 and 3. For the positively biased cycles, there were downwards plastic settlements for the spudcan on leg 1, and slight upwards movements for the spudcans on legs 2 and 3. A differential settlement of the spudcans causes a rotation $\Delta\theta_{DIFSET}$ of the jackup given by:

$$\Delta\theta_{DIFSET} = (\Delta v_1 - \Delta v_{23}) / D \qquad (9)$$

where D is the leg spacing in elevation. Figure 5 shows that D=186mm for the model in these tests. The rotation contributes a horizontal drift $\Delta h_{HULL,DIFSET}$ of the hull load reference point given by:

$$\Delta h_{HULL,DIFSET} = Y.\ \Delta\theta_{DIFSET} = (Y / D).(\Delta v_1 - \Delta v_{23}) \qquad (10)$$

where Y is the height from the spudcan load reference points (LRP's) to the hull reference point HRP at which the hull horizontal displacements are measured. As noted earlier, Y≈352mm for the model of Figure 5. In Figure 16(c), the normalised net horizontal load $H_{NET}/3A$ is plotted versus an adjusted normalised hull horizontal displacement $\Delta h^*_{HULL}/B$, where:

$$\Delta h^*_{HULL} = \Delta h_{HULL} - \Delta h_{HULL,DIFSET} \qquad (11)$$

Three results may be observed. First, the horizontal drift is virtually eliminated. Second, the hysteresis is virtually eliminated. This indicates that a major fraction of soil-related damping is associated with plastic vertical settlements. Third, normalised secant stiffnesses $(\Delta H_{NET}/3A)/(\Delta h^*_{HULL}/B)$ in Figure 16(c) can be estimated, and are around 20% higher in two-way cycling and 30% higher in positively-biased cycling than corresponding values estimated from Figure 16(a). This indicates that a significant fraction of the horizontal flexibility seen at hull level was due to plastic differential settlements of the spudcans.

3.4 Pullout

At the end of the tests, the model jackup was reloaded vertically in tests B and C. In all three tests, the model was finally unloaded and pulled out of the clay at a steady rate of upwards displacement.

Figures 17(a–c) show data for these final events. In each diagram, the normalised spudcan vertical displacement v_{SPUD}/B is plotted on the vertical axis versus the average spudcan vertical stress V_{SPUD}/A over the full spudcan area $A=\pi B^2/4$. Symbol L1 stands for the spudcan on leg 1. Symbol L23 stands for the average of the spudcans on legs 2 and 3. The vertical displacement origins are the same as those for the preloading data in Figures 8(a–c), and these data are also shown in Figures 17(a–c). The dotted lines C-C show estimates of the average stress V_{SPUD}/A at which cavitation would be expected to occur, computed as follows:

$$V_{SPUD}/A \text{ at cavitation} \approx -\{100\text{kPa} + \rho_W.G_{WS}.(1+(z_{MWS}/2R_{WS})).z_{MWS}\}. \quad (12)$$

where $\rho_W=1000\text{kg/m}^3$ is the mass density of water, G_{WS} is the centrifuge gravity at the model water surface, z_{MWS} is depth below the water surface, and R_{WS} is the radius of the water surface from the centrifuge axis. The first component, –100kPa, is an estimate of the excess pore pressure estimated to induce cavitation in the pore water when the equilibrium pressure is atmospheric. The second component takes account of the increase in hydrostatic water pressure with depth in the centrifuge model. The low fluid level in the model tests (level B in Figure 5) means that limits represented by the dotted lines C-C in Figures 17(a–c) are smaller than would have been the case for a model of a full-scale prototype in a water depth corresponding to level A in Figure 5.

The data in Figures 17(b,c) show that, in vertical reloading, the load-displacement responses moved towards, and became continuations of, the previous elasto-plastic preloading curves. This suggests that plastic damage to the soil during the previous cyclic loading events listed in Table 4 may haven been partially erased by sufficient additional settlements under pure vertical load. However, the yield points marked "X" in Figures 17(b,c) are less sharp than the yield points at the end of the unloading-reloading excursions in the preloading phases of the tests.

On vertical unloading, the data show marked changes of response associated with the change of vertical spudcan load V_{SPUD} from positive to negative. The times at model and prototype scale from the time of this change to the times when the spudcans broke away from the soil are listed in the diagrams. Some water may have been sucked into the soil over these time periods. In all cases, breakout began at values of V_{SPUD}/A less than estimated cavitation limits. Further analysis or experiments would be needed to determine whether breakout stresses would have been larger if the fluid surface in the model tests had been at level A in Figure 5, rather than level B.

4. Conclusions

This paper has reported and discussed centrifuge test data of models of three-leg jackups on kaolin clay. The tests modelled one prototype jackup with 6.5 metre diameter 13º conical spudcans, one with 6.5 metre diameter flat-based spudcans, and one with 13.0 metre diameter flat-based spudcans.

The vertical preloading data confirmed that large vertical plastic settlements were required to attain significant vertical strength. Results for the flat-based spudcans indicated that the vertical spudcan stress V_{SPUD}/A required to achieve a given prototype penetration v_{SPUD} would be sensibly the same for a 6.5 metre diameter spudcan as for a 13.0 metre diameter spudcan.

The data of slow cyclic horizontal loading showed significant hysteresis in the hull horizontal load-displacement responses. Secant horizontal stiffnesses were larger when the jackup was fitted with 13° conical spudcans compared to flat spudcans of the same diameter. Spudcan loadpaths indicated that responses were close to pinned. Spudcan horizontal load-displacement and moment-rotation responses

showed marked hysteresis and plasticity. In these tests, the spudcans on legs 2 and 3 generally took a larger share of changes of horizontal load and experienced larger changes of moment compared to the spudcan on leg 1, for both spudcan shapes and both sizes. A bias developed in the moment responses, with the spudcan on leg 1 appearing to become incapable of sustaining significant positive moment, and the spudcans on legs 2 and 3 appearing to become incapable of sustaining significant negative moments.

The data of rapid cyclic horizontal loading indicated that there may be thresholds below which significant spudcan vertical displacement do not occur. Threshold values will depend on a variety of factors including rig geometry and size and soil characteristics. Differential spudcan settlements had three effects. They were largely responsible for an apparent horizontal drift of the hull in two-way cycling and in positively-biased one-way cycling. They increased the amount of energy absorbed during individual cycles, leading to increased overall damping. They decreased the secant horizontal stiffnesses seen at hull level.

In the final events, it was found that vertical re-loading responses moved towards, and became continuations of, the previous preloading curves. This suggests that settlements associated with pure vertical reloading may erase effects of prior cyclic loading. During pullout, significant changes of response occurred as the spudcan loads V_{SPUD} changed from compressive to tensile. Breakout occurred at average spudcan vertical stresses that were less than the estimated cavitation-limited stresses. It is not possible to know from these data whether higher breakout loads might have been achieved if the cavitation limits had been higher.

Acknowledgements

The tests reported here were part of a series of tests on sand and clay soils funded by Esso Exploration and Production UK Limited (EEPUK) and carried out with the help of staff of Andrew N Schofield & Associates Limited at Cambridge University's Geotechnical Centrifuge Centre. Dr R.Phillips, now at the Centre for Cold Ocean Resources Engineering, advised on the clay specimen preparation. We would also like to thank N.R.Sosdian of EEPUK and J.D.Murff and P.C.Wong of Exxon Production Research Company. Opinions in this paper do not necessarily represent opinions of the acknowledgees or organisations involved.

References

1. Ahrendesen, B.K., Dutt, R.N., and Ingram, W.B., 1989, "Jackup footing performance: an integrated approach to geotechnical assessment", Paper OTC *6027, Offshore Technology Conference*

2. Airey, D.W., 1984, "Clays in simple shear apparatus", Ph.D thesis, Cambridge University

3. Almeida, M.S.S., 1984, "Staged construction of embankments on soft clay", Ph.D thesis, Cambridge University

4. Al-Tabbaa, A., 1984, "Anisotropy of clay", M.Phil thesis, Cambridge University

5. Al-Tabbaa, A., 1987, "Permeability and stress-strain response of speswhite kaolin", Ph.D thesis, Cambridge University

6. Al-Tabbaa, A., and Wood, D.M., 1987, "Some measurements of the permeability of kaolin", *Geotechnique,* 37(4), *499-503*

7. Arnesen, K., Dahlberg, R., Hjesy, K., and Karlsen, C.A., 1988, "Soil-structure interaction aspects for jackup platforms", *Behaviour of Offshore Structures,* BOSS 88, eds T.Moan, N.Janbu, and O.Faltinsen, Tapir Publishers, Trondheim, Vol. 1, 259-277

8. Asquer, P.F., and Antalovsky, S.A. 1982, "Rig jacking on soft soil foundations: improvements in safety and speed by monitoring leg loads", Paper OTC 4408, *Offshore Technology Conference*

9. Baglioni, V.P., Chow, G.S., and Endley, S.N., 1982, "Jackup rig foundation stability in stratified soil deposits", Paper OTC 4409, *Offshore Technology Conference*

10. Boswell, L.F. (ed), *1986, The Jackup Drilling Platform,* Collins

11. Boswell, L.F., and D'Mello, *C.,* (eds), 1993, *The Jackup Platform: Design, Construction, and Operation,* Proc 4th Int Conf, Bentham Press, London

12. Boswell, L.F., and D'Mello, *C.,* (eds), 1995, *The Jackup Platform: Design, Construction, and Operation,* Proc 5th Int Conf, Bentham Press, London

13. Brekke, J.N., Murff, J.D.,Campbell, R.B., and Lamb, W.C., 1989, "Calibration of a jackup leg foundation model using full-scale structural measurements", Paper OTC 6127, *Offshore Technology Conference*

14. Chaney, R.C., and Demars, K.R., 1991, "Offshore Structure Foundations", Chapter 18 of Foundation Engineering Handbook, Second Edition, ed.H-Y. Fang, Chapman & Hall, 679-734

15. Clegg, D., 1981, "Model piles in stiff clay", Ph.D thesis, Cambridge University

16. Corte, J-F., (ed), 1988, Centrifuge 88, Proc Int Conf Geotechnical Centrifuge Modelling, Balkema

17. Craig, W.H., 1983, "Simulation of foundations for offshore structures using centrifuge modelling", *Developments in Soil Mechanics and Foundation Engineering – I, Model Studies,* eds.P.K.Banerjee and R.Butterfield, Applied Science Publishers, Chapter 1, 1-27

18. Craig, W.H., (ed), 1984, *Application of Centrifuge Modeling Techniques to Geotechnical Design,* Balkema

19. Craig, W.H., and Chua, K., 1991, "Large displacement performance of jackup spudcans", *Centrifuge* 97, eds.H-Y.Ko and F.G.McLean, Balkema, 139-144

20. Craig, W.H., James, R.G., and Schofield, A.N., (eds), 1988, *Centrifuges in Soil Mechanics,* Balkema

21. Dean, E.T.R., James, R.G., Schofield, A.N., Tan, F.S.C., and Tsukamoto, Y., 1992, "Combined vertical, horizontal, and moment loading of circular spuds on dense sand foundations: Data report for drum centrifuge tests YT1–1 L-A thru -G and YT2–1L–G thru –Y", Technical Report CUED/D–Soils/TR244, Cambridge University Engineering Department

22. Elmes, D., 1986, "Creep and viscocity in two kaolin clays", Ph.D thesis, Cambridge University

23. Endley, S.N., Rapoport, V., Thompson, P.J., and Baglioni, V.P., 1981, "Prediction of jackup rig footing penetration", Paper OTC 4144, *Offshore Technology Conference*

24. Fujii, T., Kobayashi, T., and Tagaya, K., 1989, "Punchthrough encountered in India and Indonesia", Paper OTC 6124, *Offshore Technology Conference*

25. Hambly, E.C., 1990, "Overturning Instability", *ASCE Journal of Geotechnical Engineering,* 116(4), 704-709

26. Hambly, EC., and Nicholson, B.A., 1991, "Jackup dynamic stability under extreme storm conditions", Paper OTC 6590, *Offshore Technology Conference*

27. Hambly, E.C., Imm, G.R., and Stahl, B., 1990, "Jackup performance and foundation fixity under developing storm conditions", Paper OTC 6466, Offshore Technology Conference

28. Houlsby, G.T., and Martin, C.M., 1992, "Modelling the behaviour of foundations of jackup units on clay", *Predictive Soil Mechanics,* Proc Wroth Mem Symp, Thomas Telford, 339-358

29. Knoyle, D.S., 1979, "The influence of pore-water tension on the undrained shear strength of kaolin", Part III Project Report, Cambridge University Engineering Department

30. Ko, H-Y., and McLean, F.G., (eds), 1991, *Centrifuge* 91, Proc Int Conf Geotechnical Centrifuge Modelling, Balkema

31. Leung, C.F., Lee, F.H., and Tan, G.T.S., 1994, *Centrifuge* 94, Proc Int Conf Geotechnical Centrifuge Modelling, Balkema

32. Martin, C.M., 1991, "The behaviour of jackup rig foundations on clay", First Year Research Report, Department of Engineering Science, Oxford University

33. Martin, C.M., and Houlsby, G.T., 1994, "Combined loading tests of scale model spudcan footings on soft clay: experimental data", Technical Report 2029/94, Department of Engineering Science, Oxford University

34. McClelland, B., Young, A.G., and Remmes, B.D., 1982, "Avoiding jackup rig foundation failures", *Geotechnical Engineering,* 13, 151-l 88; also *Proc Syrnp Geotechnical Aspects of Offshore and Nearshore Structures,* Balkema

35. McNeilan, T.W. and Bugno, W.T., 1985, "Jackup rig performance in predominantly silty soils", Paper OTC *5082, Offshore Technology Conference*

36. Osborne, J.J., Trickey, J.C., Houlsby, G.T., and James, R.G., 1991, "Findings from a joint industry study on foundation fixity of jackup units", Paper OTC 6615, *Offshore Technology Conference*

37. Phillips, R., 1989, "Centrifuge lateral pile tests in clay (Exhibit PR-10592), Task 1 - Final Report", Report by Lynxvale Limited to Exxon Production Research Company

38. Poulos, H.G., 1988, *Marine Geotechnics,* Unwin Hyman

39. Reardon, M.J., 1986, "Review of the geotechnical aspects of jackup unit operations", *Ground Engineering,* Vol.1 9, No.7

40. Rowe, P.W., 1975, "Displacements and failure modes of model offshore gravity platforms founded on clay", *Proc Offshore Europe '75*

41. Rowe, P.W., 1983, "Use of large centrifugal models for offshore and nearshore works", *Proc Int Symp Geotechnical Aspects of Coastal and Offshore Structures,* Bangkok, eds.Yudbhir and A.S.Balasubrananiam, Balkema, 21-33

42. Rowe, P.W., Craig, W.H., and Procter, D.C., 1976, "Model studies of offshore gravity structures founded on clay", Behaviour of Offshore Structures BOSS 76, Vol. 1, 439-448

43. Santa Maria, P.E.L.de, 1988, "Behaviour of footings for offshore structures under combined loading", Ph.D thesis, Oxford University

44. Schofield, A.N., 1980, "Cambridge geotechnical centrifuge operations", *Geotechnique,* 30(3), *227-268*

45. Schofield, A.N., 1981, "Dynamic and earthquake geotechnical centrifuge modelling", *Proc Int Conf Recent Advances in Soil Dynamics and Earthquake Engineering,* Missouri

46. Senner, D.W.F., 1992, "Analysis of long-term jackup rig foundation performance", *Offshore Site Inves tiga tion and Foundation Behaviour,* eds.D.A.Ardus, D.Clare, A.Hill, R.Hobbs, R.J.Jardine, and J.M.Squire, Society for Underwater Technology, Kluwer Academic Publishers, 691-716

47. Siciliano, R.J., Hamilton, J.M., Murff, J.D., and Phillips, R., 1990, "Effect of jackup spudcans on piles", Paper OTC *6467, Offshore Technology Conference*

48. SNAME, *1994, Site Specific Assessment of Mobile Jackup Units,* Technical and Research Bulletin 5–5A, Society of Naval Architects and Marine Engineers, Jersey City, NJ

49. Springett, C.N., Stonor, R.W.P., and Wu, X., 1993, "Results of a jackup measurement programme in the North Sea and the comparison with the structural analysis", *Proc 4th Int Conf The Jackup Platform,* eds.L.F.Boswell and C.D'Mello, Bentham Press, London

50. Springman, S.M., 1993, "Centrifuge modelling in clay marine applications", Keynote Address, 4th Canadian Marine Geotechnical Conference, St.Johns, Newfoundland

51. Stewart, W.P., White, R.M., Rapoport, V., and Devoy, S.D., 1989, "On-bottom stability of jackups", Paper OTC *6125, Offshore Technology Conference*

52. Stewart, W.P., Rapoport, V., and Oser, M., 1991, "Observed storm stability of jackup boats (liftboats)", Paper OTC 6611, Offshore Technology *Conference*

53. Tan, F.S.C., 1990, "Centrifuge and theoretical modelling of conical footings on sand", Ph.D thesis, Cambridge University

54. Taylor, R.N., (ed), 1994, *Geotechnical Centrifuge* Technology, Blackie Academic & Scientific

55. Wong, P.C., Chao, J.C., Murff, J.D., Dean, E.T.R., James, R.G., and Schofield, A.N., 1993, "Jackup rig foundation modeling II", Paper OTC *7303, Offshore Technology Conference*

56. Young, A.G., Remmes, B.D., and Meyer, B.J., 1984, "Foundation performance of offshore jackup rig drilling ships", *ASCE Journal of Geotechnical Engineering, 11* 0(7), *841-859*

Table 1. Some Material Properties of Speswhite Kaolin

Specific Gravity G_S	2.61	Clegg (1981), Elmes (1986)
	2.64	Al-Tabbaa (1984)
MC at Plastic and Liquid Limits	38%, 69%	Clegg (1981), Airey (1984)
	31%, 64%	Phillips (1989)
K_o, normally consolidated	0.69	Airey (1984), Al-Tabbaa (1984)
Critical state stress ratio M	0.9(comp), 0.68(ext)	Al-Tabbaa (1984)
	0.82 (comp)	Elmes (1986)
Critical state model, λ	0.31-0.21	Airey (1984)
	0.14	Elmes (1986)
	0.187	Al-Tabbaa (1987), Phillips (1989)
Critical State model, κ	0.03	Elmes (1986)
	0.03-0.06	Al-Tabbaa (1987)
Critical state model, Γ	3.44	Clegg (1981)
	2.87	Elmes (1986)
	3.00	Al-Tabbaa (1987)
c_u, isotropically consolidated	$0.23p'_{max}$	Clegg (1981)

Permeability of 1 D consolidated samples at specific volume V=l +voids ratio :

vertical direction	$0.53\ (V\text{-}l)^{3.16} \times 10^{-6}$ mm/sec	Al-Tabbaa and Wood (1987)
	$0.34\text{-}2.9 \times 10^{-6}$ mm/sec	Springman (1993)
horizontal direction	$1.49\ (V-1)^{2.03} \times 10^{-6}$ mm/sec	Al-Tabbaa and Wood (1987)

The clay specimens were created by mixing kaolin powder with de-ionised water. The powder was obtained from English China Clays PLC, St.Austell, Cornwall. Parameter variations may be due to differences between batches over time, and/or to different methods of fitting straight lines to curved data over different ranges of stress or specific volume, etc.

Table 2. Summary of Jackup Model Tests on Clay

Test	A	B	C
Spudcan shape	13° cones	flats	flats
Nominal gravity G_{NOM}	128g	128g	256g
Scale factor $N = 0.88G_{NOM}/g$	113	113	225
Prototype spudcan diameter Bp	6.5 metres	6.5 metres	13.0 metres
Cyclic loading event numbers	2-8	2-8	2-9

Table 3. Scaling Relations *

Length, displacement	prototype = N x model
Area	prototype = N^2 x model
Section Modulus Z_e	prototype = N^3 x model
Flexural rigidity El	prototype = N^4 x model
Non-dimensional displacement (e.g.v/B)	prototype = model
Angle, rotation	prototype = model
Effective stress, strain, excess pore pressure	prototype = model
Soil modulus (stress/strain)	prototype = model
Force	prototype = N^2 x model
Moment	prototype = N^3 x model
Coefficients of consolidation, cv, c_H	prototype = model
Consolidation and drainage time	prototype = N^2 x model
Consolidation time factor $T=c_V t/B^2$	prototype = model

* The scaling relation for distance implies that, to model a prototype jackup in a full design water depth, the model fluid surface would have had to be around level A in Figure 5. The lower model water surface, at level B, had no effect on the scaling laws during the periods in which cavitation did not occur in the pore fluid.

Table 4. Cyclic Horizontal loading events at model and prototype scales

Test	Event No.	Description	$H_{NET}/3A$, kPa max.neg	max.pos	T_M/cycle seconds	T_P/cycle days
A	2	Rapid, 2-way	− 8.4	+ 7.5	8.8	1.3
B	2	Rapid, 2-way	− 5.2	+ 5.4	8.8	1.3
c	2	Rapid, 2-way	− 5.3	+ 4.6	9.7	5.7
A	3	Slow, 2-way	− 11.0	+ 9.2	90	13.3
B	3	Slow, 2-way	− 9.6	+ 9.3	80	11.8
C	3	Slow, 2-way	− 8.3	+ 6.9	125	73
A	4	Rapid, 1 -way, negative	− 9.6	+ 2.5	8.8	1.3
B	4	Rapid, 1 -way, negative	− 5.8	+ 1.1	8.8	1.3
C	4	Rapid, 1 -way, negative	− 6.4	+ 2.4	10	5.9
A	5	Slow, l-way, negative	− 15.2	+ 0.3	65	9.6
B	5	Slow, 1 -way, negative	− 11.2	+ 1.3 *	65	9.6
C	5	Slow, l-way, negative	− 11.0	+0.7	80	47
A	6	Rapid, l-way, positive	− 2.6	+ 6.8	8.8	1.3
B	6	Rapid, 1 -way, positive	− 2.0	+ 4.5	8.8	1.3
C	6	Rapid, l-way, positive	− 2.1	+ 5.1	10	5.9
A	7	Slow, 1 -way, positive	− 4.0	+ 12.8	60	8.9
B	7	Slow, 1 -way, positive	− 2.4	+ 10.8	80	11.8
C	7	Slow, 1 -way, positive	− 2.7	+ 8.9	80	47
A	8	Slow, 1 -way, negative	− 16.6	+ 0.0	30	4.4
B	8	Rapid, 2-way	− 7.2	+ 6.6	8.8	1.3
C	8	Rapid, 2-way	− 11.7	+ 8.7	10	5.9
C	9	Slow, 2-way	− 19.2	+ 11.6	180	105

* event 5 of test B ended with one l-way positive cycle to $H_{NET}/3A$=+11.2kPa

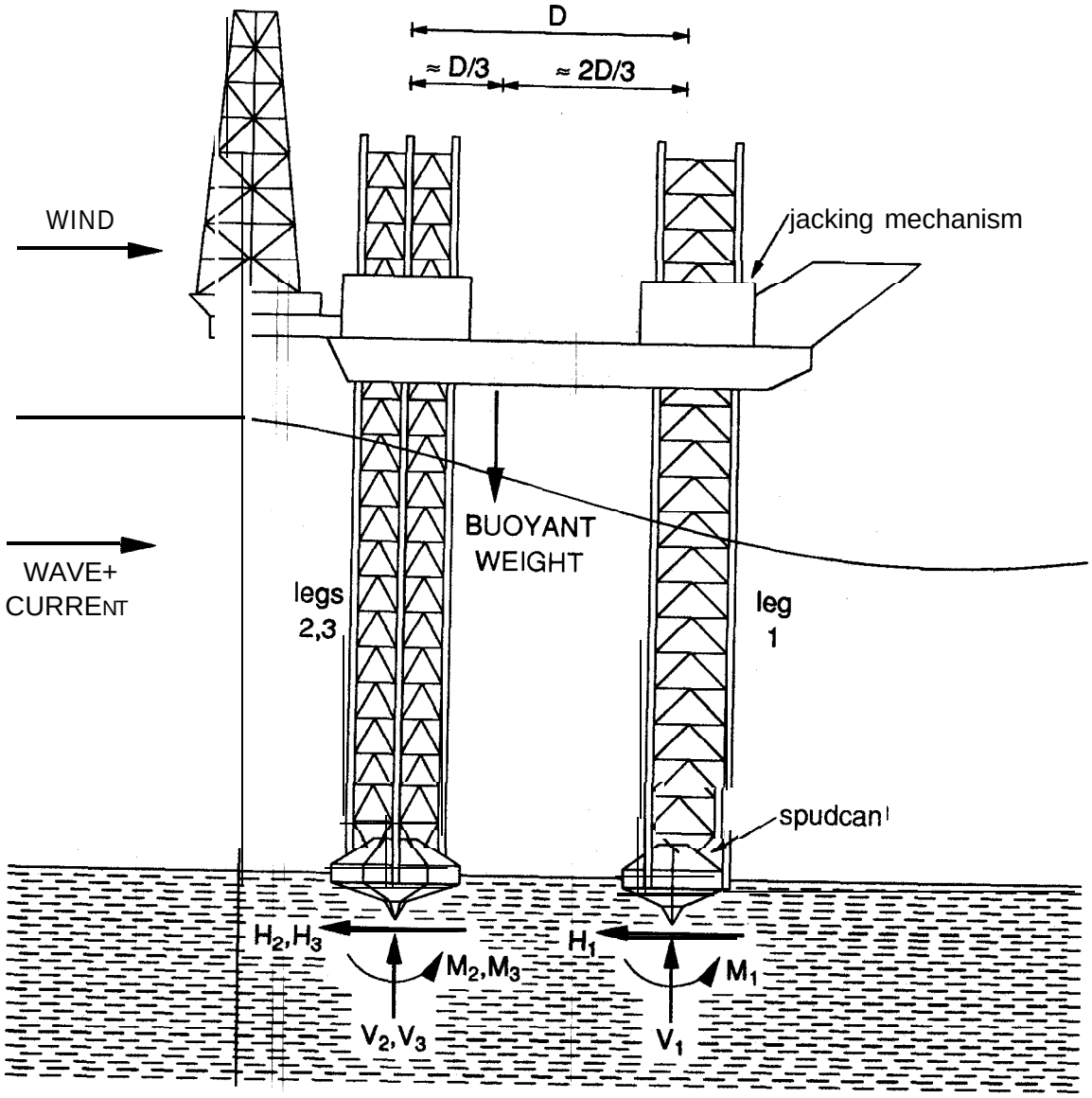

CUED
L-Soils/
TR289

THREE-LEG JACKUP

FIG.NO.

1

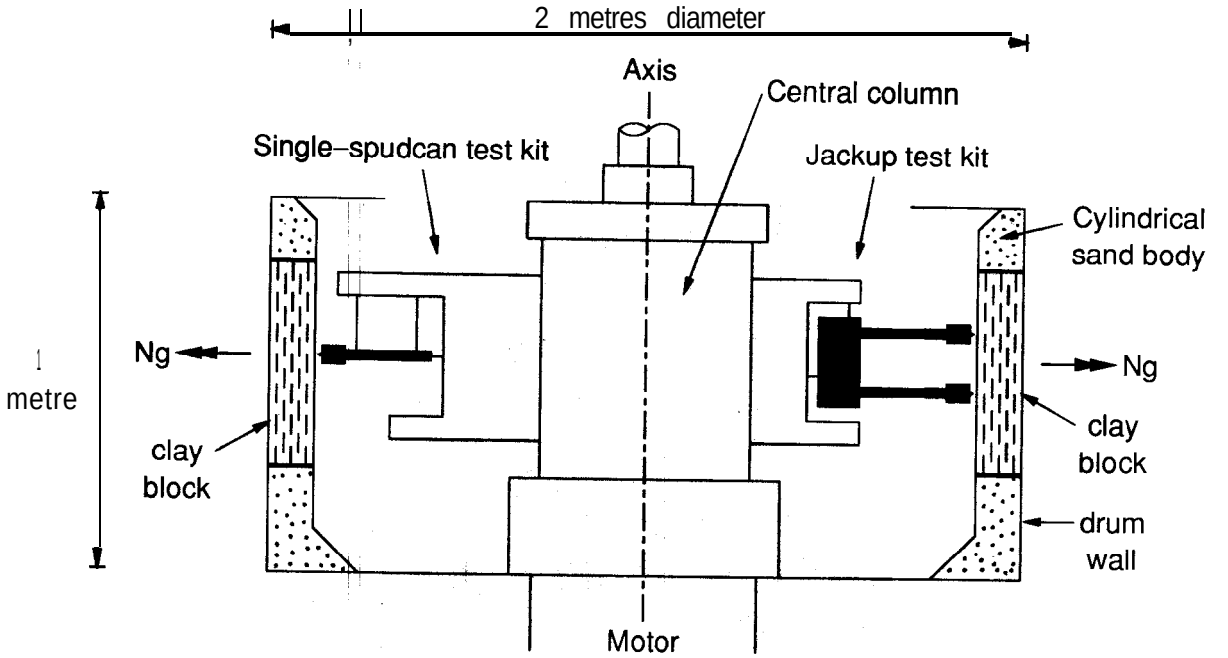

(a) elevation view

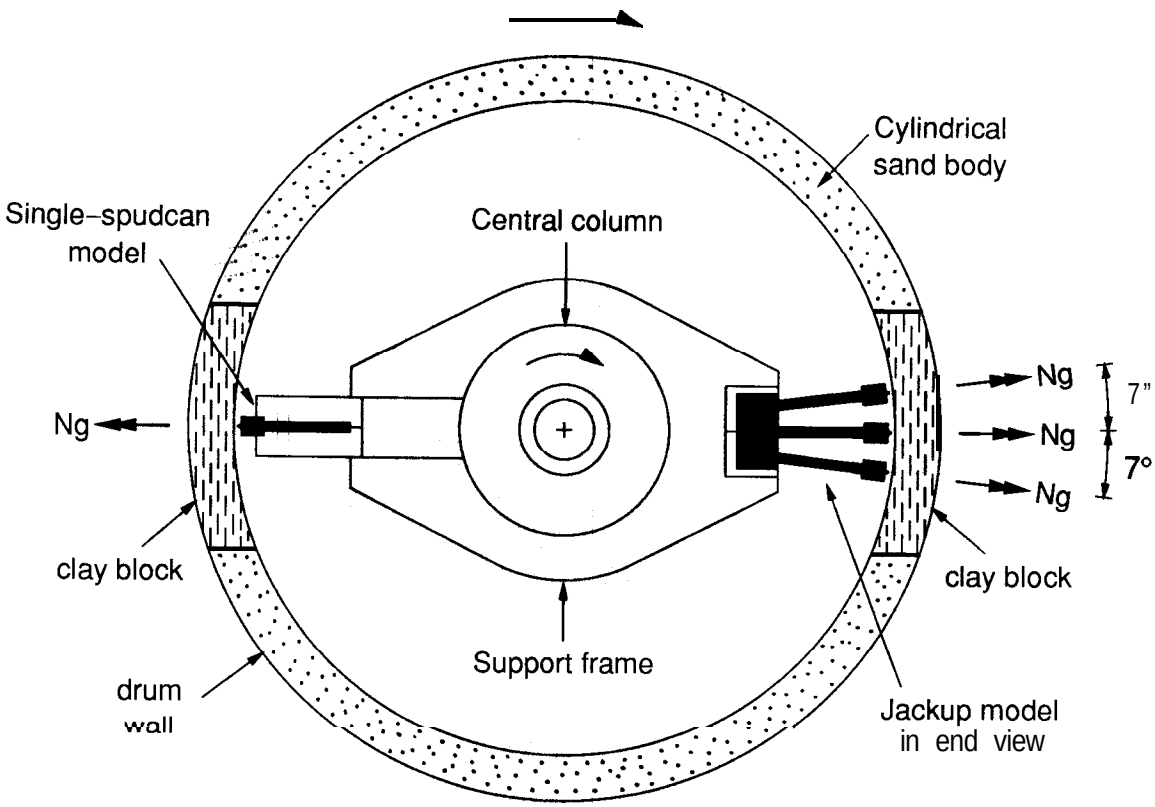

(b) plan view

CUED ID-Soils/ TR289	CAMBRIDGE 2-METRE DRUM CENTRIFUGE CONFIGURED FOR JACKUP/SPUDCAN TESTS ON OVER-CONSOLIDATED CLAY	FIG.NO. 2

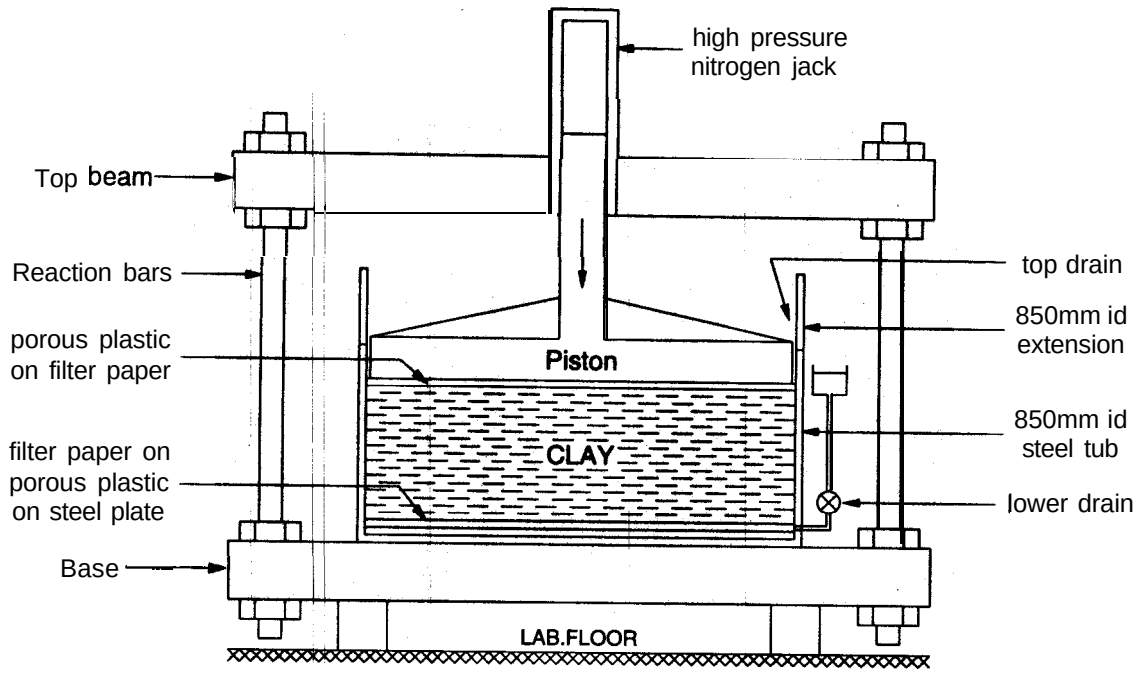

(a) consolidation in 850mm diameter steel tub

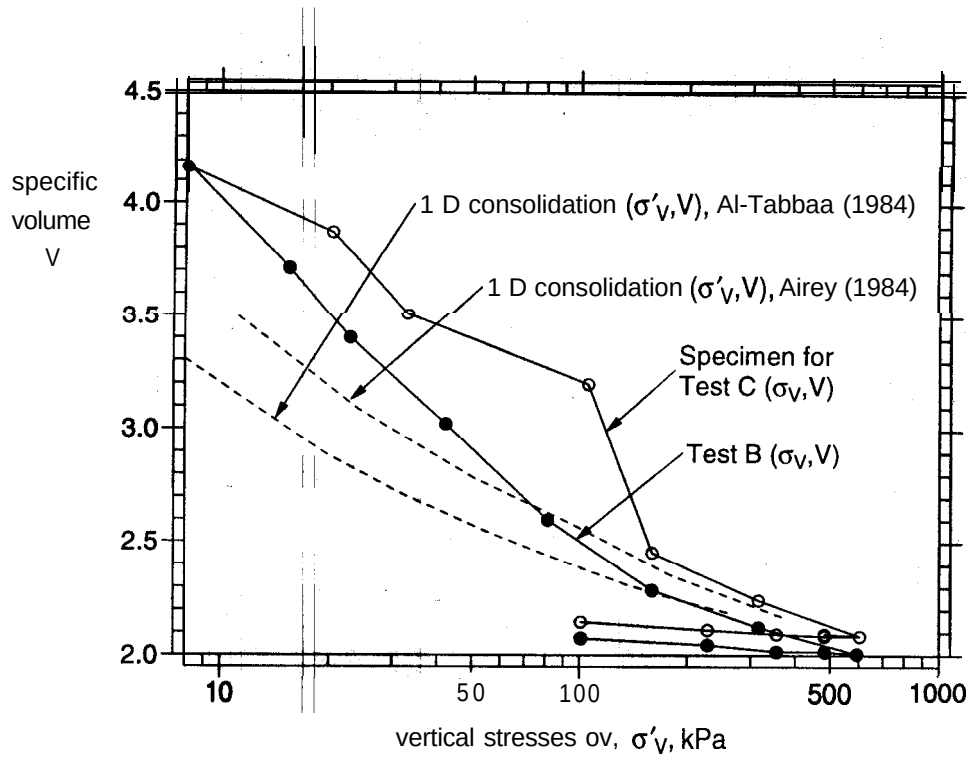

(b) specific volume and vertical stresses

CUED /D-Soils/ TR289	FIRST STAGE OF PREPARATION OF A CLAY BLOCK	FIG.NO. 3

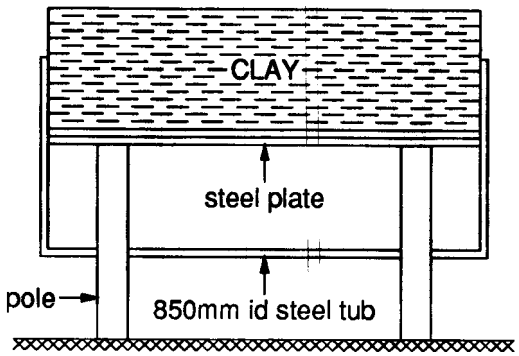

(a) extrusion from 850mm diameter steel tub

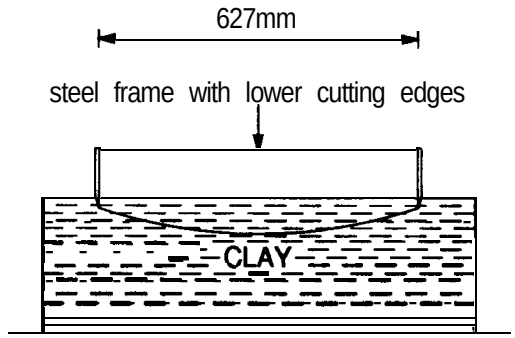

(b) cutting a block

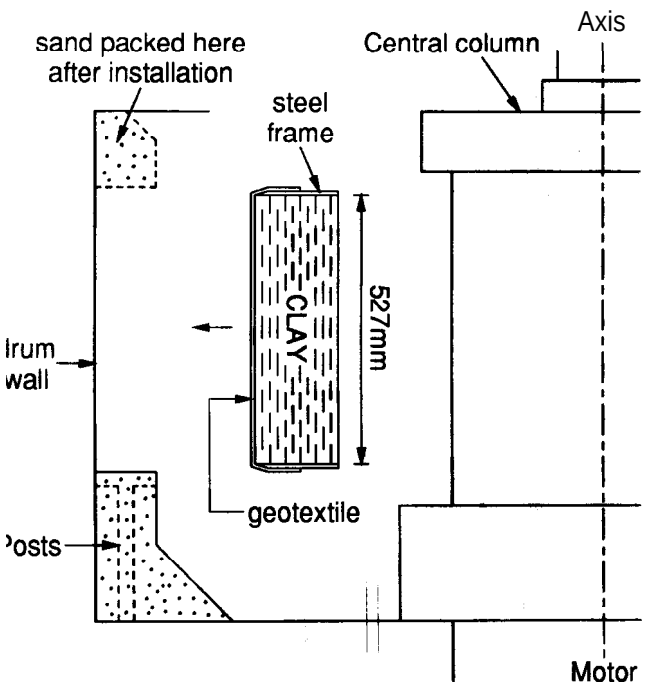

(c) installation in centrifuge

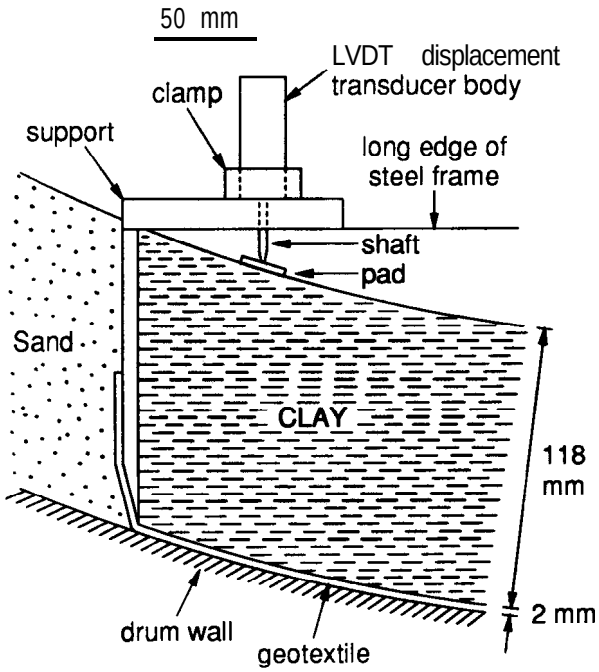

(d) settlement gauge fitted after machining inner surface

CUED D-Soils/ TR289	SECOND STAGE OF PREPARATION OF A CLAY BLOCK	FIG.NO. 4

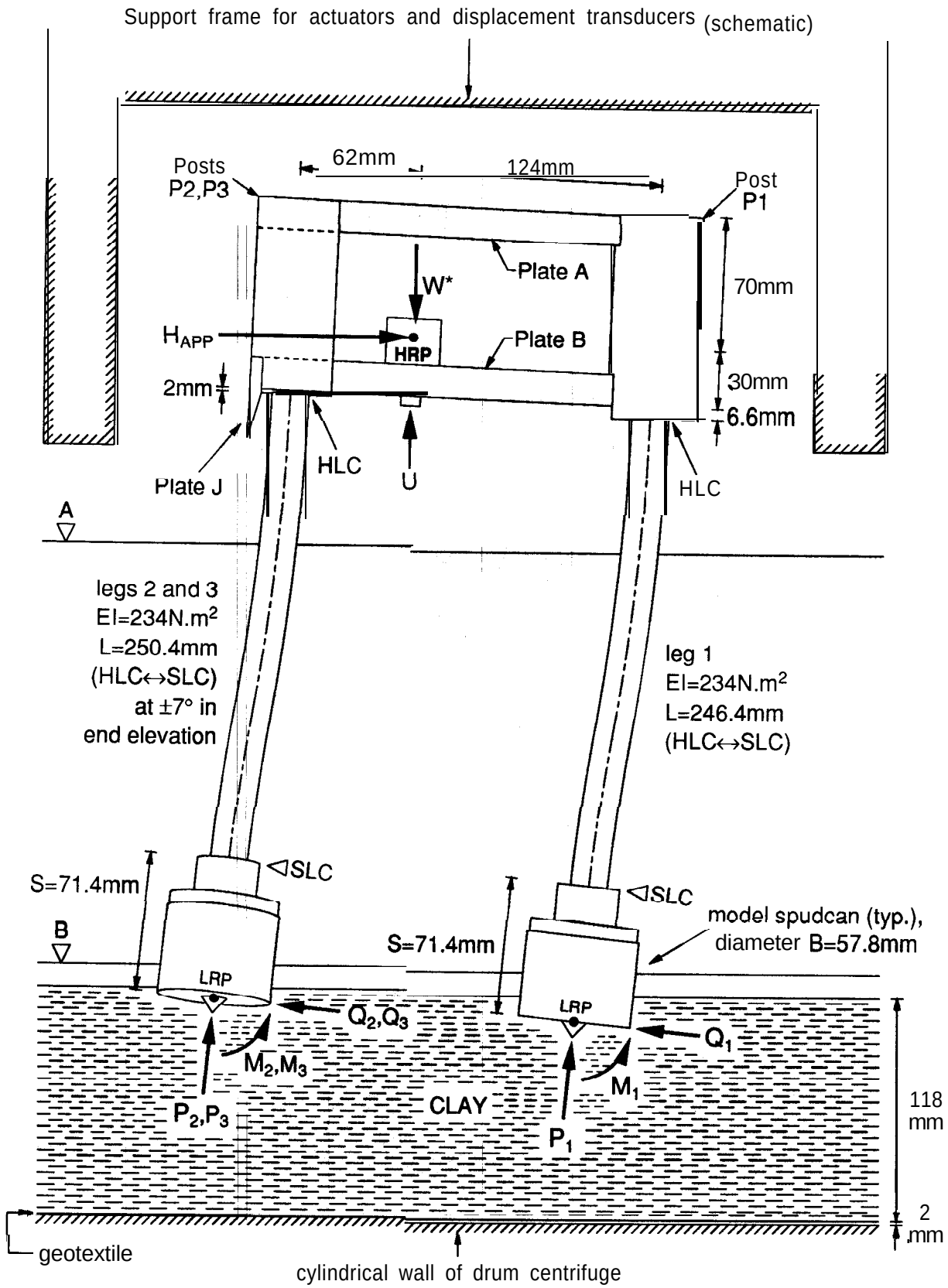

CUED 'D-Soils! TR289	3-LEG MODEL JACKUP AND SUPPORT FRAME, MODEL PROPERTIES, DIRECTIONS OF POSITIVE LOADS H_{APP}, W*, AND U, AND DIRECTIONS OF POSITIVE SOIL REACTIONS Pi, Q_i, AND M_i	FIG.NO. 5

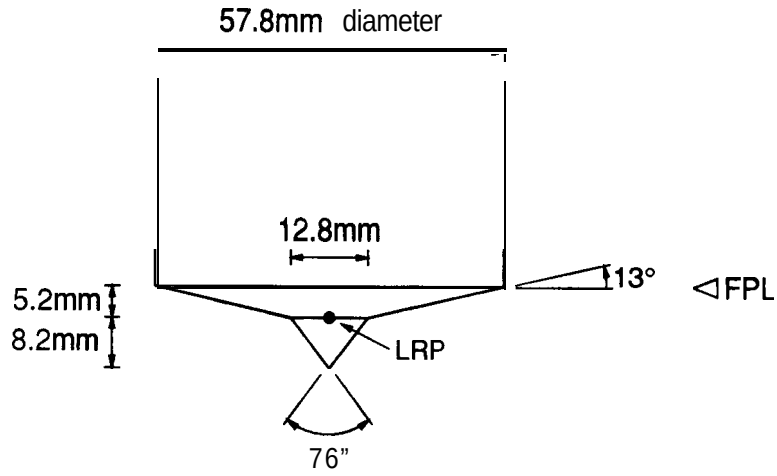

(a) 13° conical spudcans used in test A

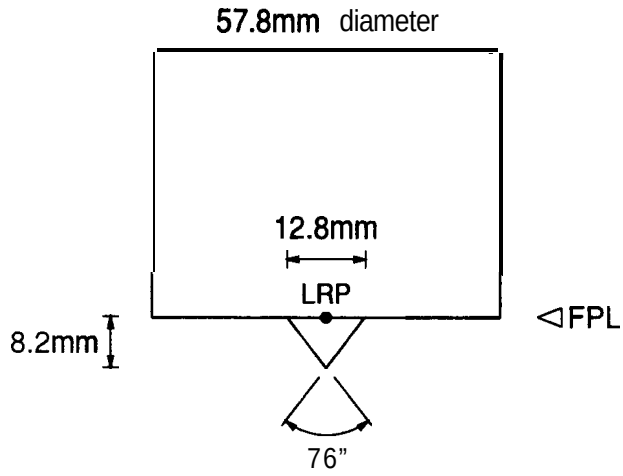

(b) flat spudcans used in tests B and C

CUED /D-Soils/ TR289	MODEL SPUDCAN SHAPES	FIG.NO. 6

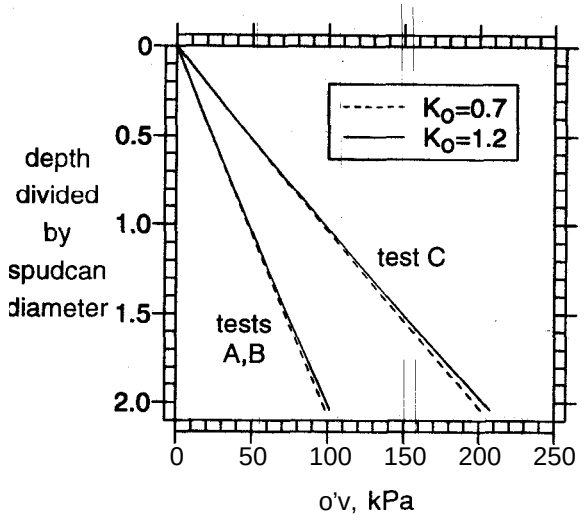

(a) in-test in-situ vertical effective stresses

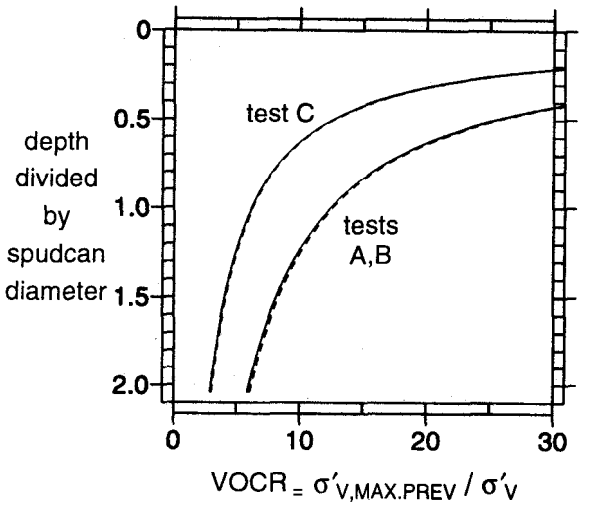

(b) vertical over-consolidation ratios

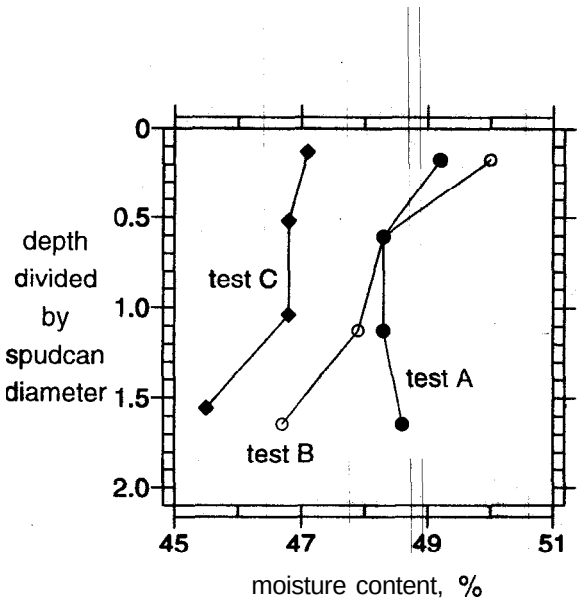

(c) post-test 1 g moisture contents

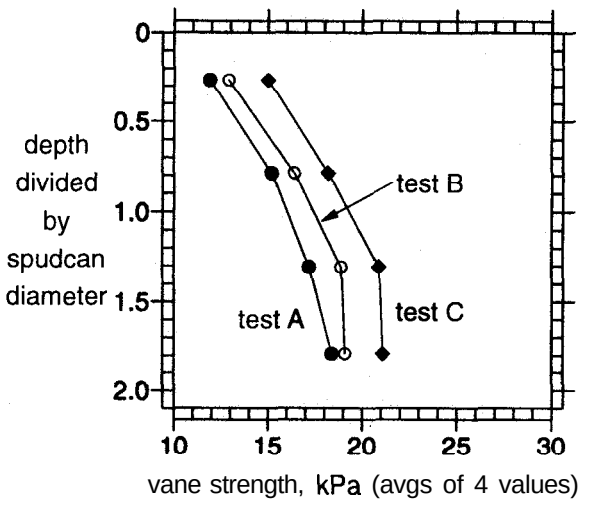

(d) post–test 1 g vane strengths

CUED /D-Soils/ TR289	ESTIMATES OF SOME IN-SITU PROPERTIES	FIG.NO. 7

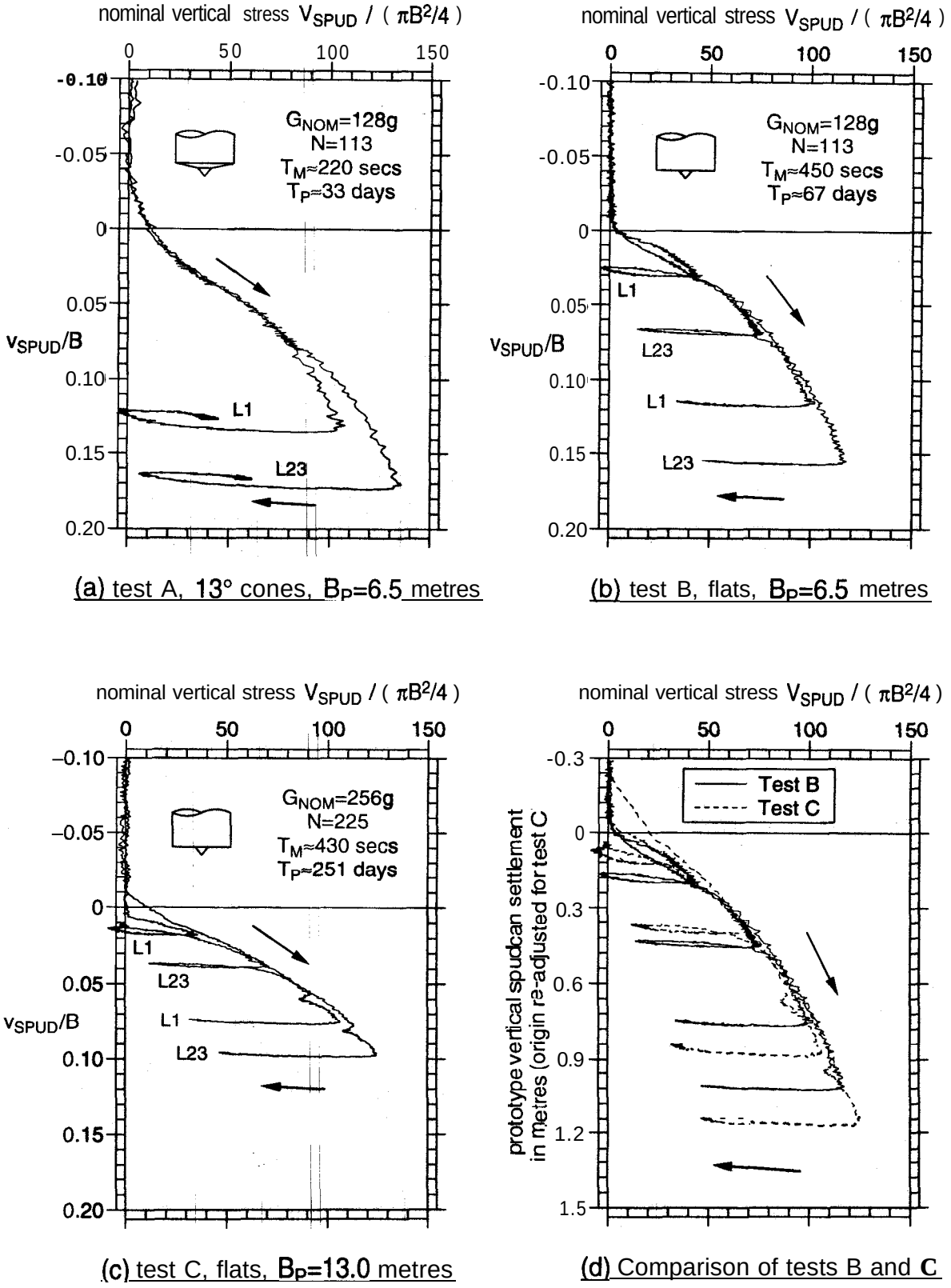

(a) test A, 13° cones, B_P=6.5 metres

(b) test B, flats, B_P=6.5 metres

(c) test C, flats, B_P=13.0 metres

(d) Comparison of tests B and C

CUED /D-Soils/ TR289	PRELOADING DATA	FIG.NO. 8

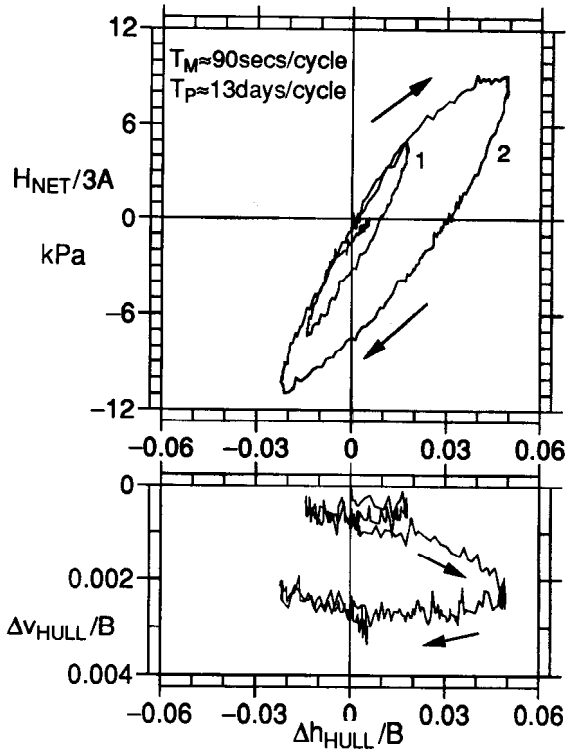

(a) test A, 13° cones, B_P=6.5 metres

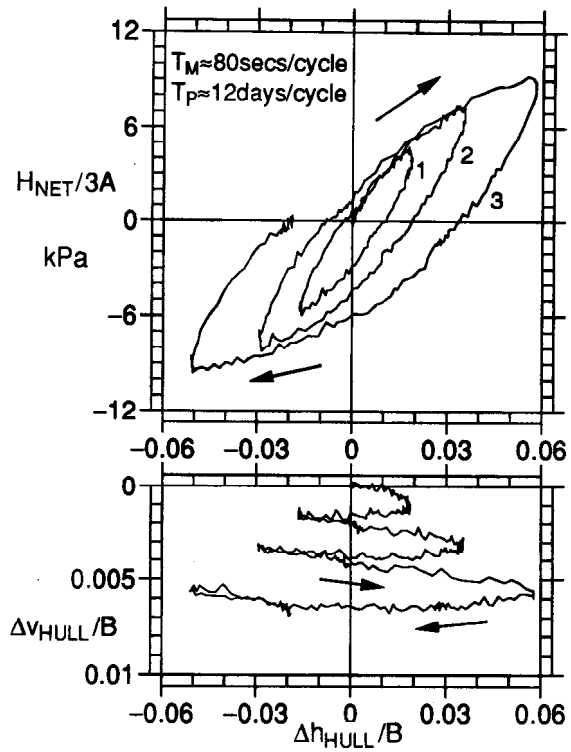

(b) test B, flats, B_P=6.5 metres

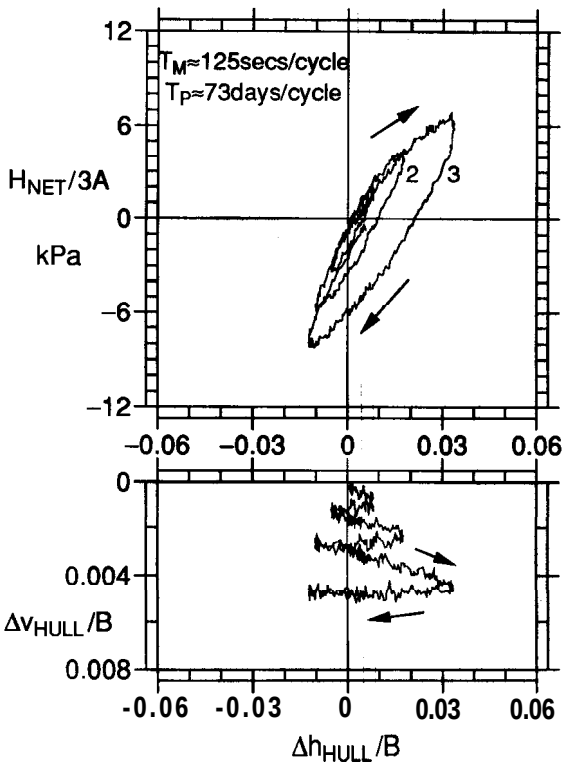

(c) test C, flats, B_P=13.0 metres

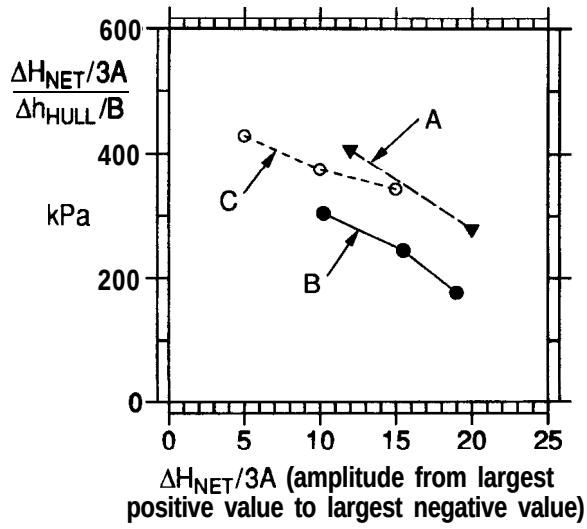

(d) comparison of normalised secant horizontal stiffnesses

CUED /D-Soils/ TR289	EVENTS N0.3. SLOW TWO-WAY CYCLING. HULL RESPONSES	FIG.NO. 9

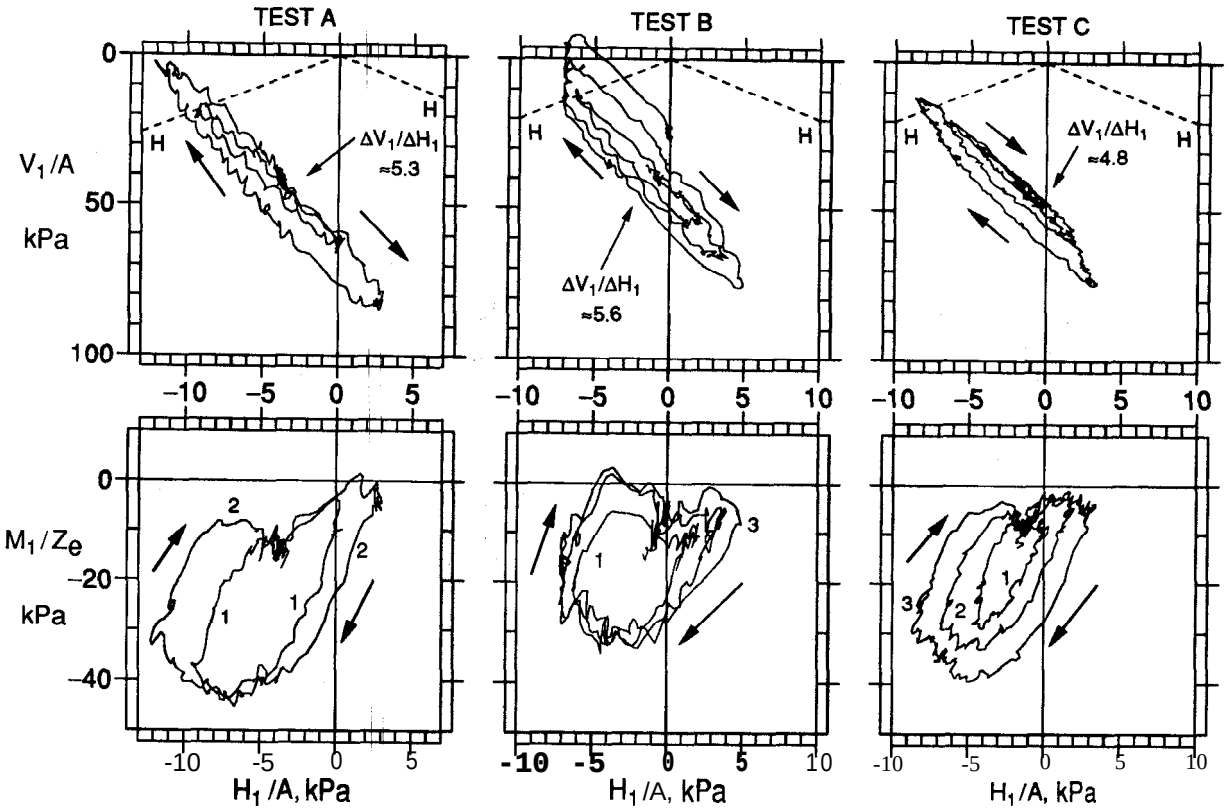

(a) Loadpaths at the spudcan on leg 1

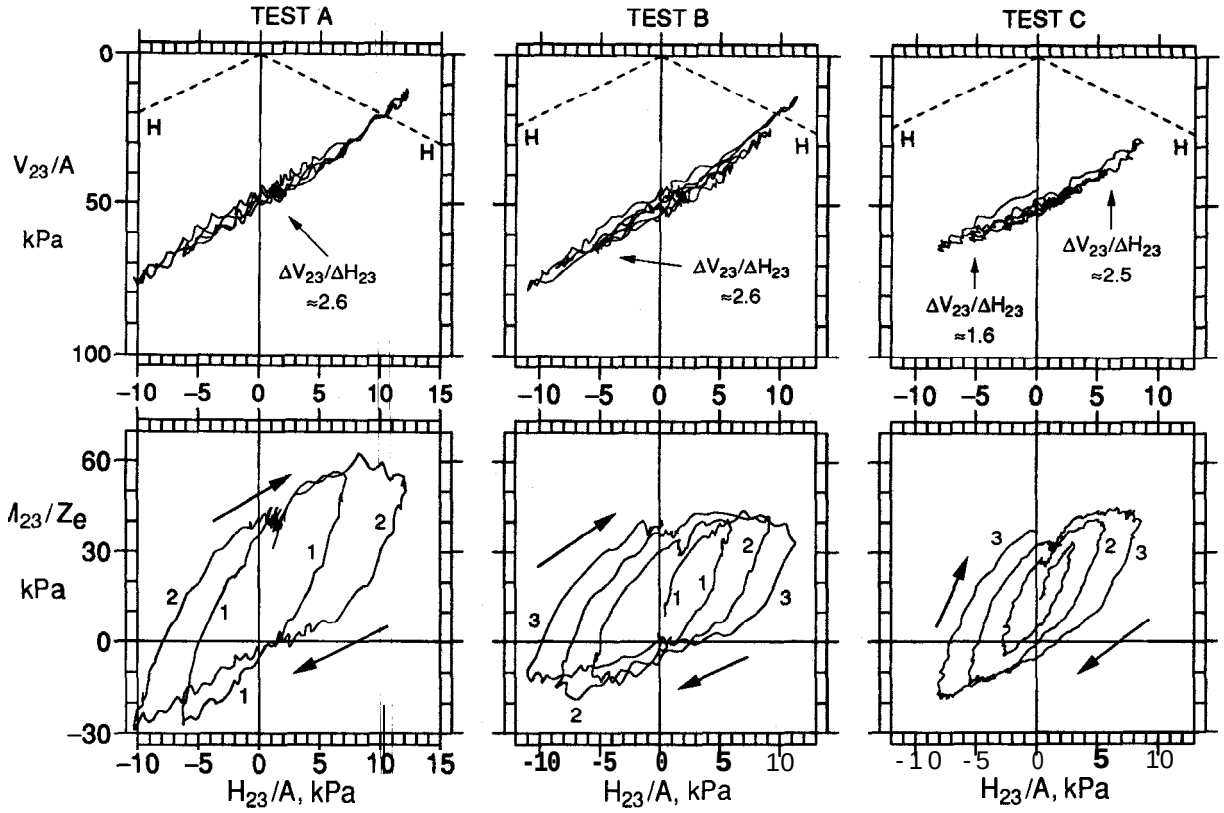

(b) Averages of loadpaths at the spudcans on legs 2 and 3

CUED /D-Soils/ TR289	EVENTS N0.3. SPUDCAN LOADPATHS	FIG.NO. 10

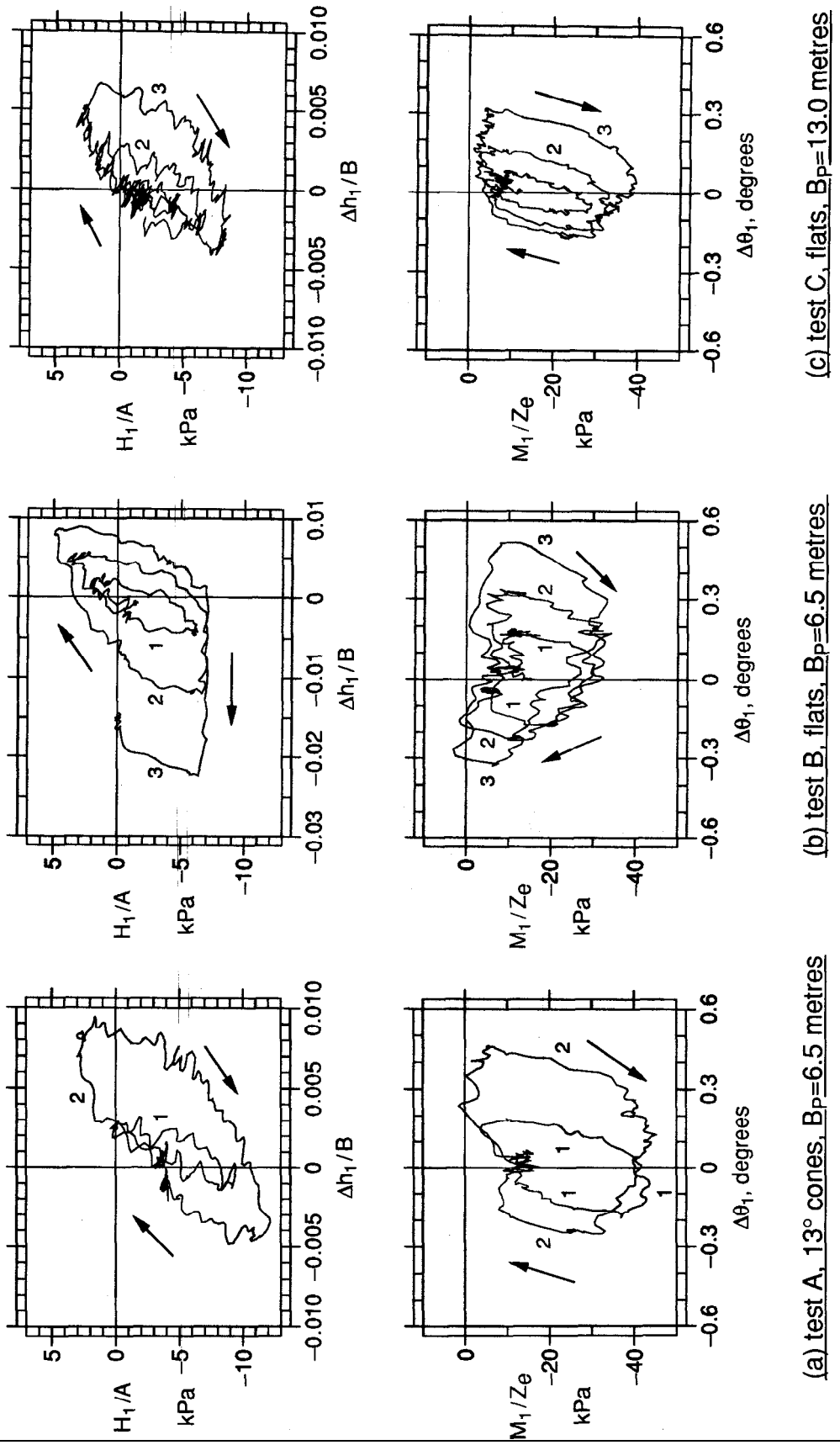

(a) test A, 13° cones, B_P=6.5 metres (b) test B, flats, B_P=6.5 metres (c) test C, flats, B_P=13.0 metres

CUED ID-Soils/ TR299	EVENTS N0.3. HORIZONTAL DISPLACEMENTS AND ROTATIONS AT THE SPUDCAN ON LEG 1	FIG.NO. 11

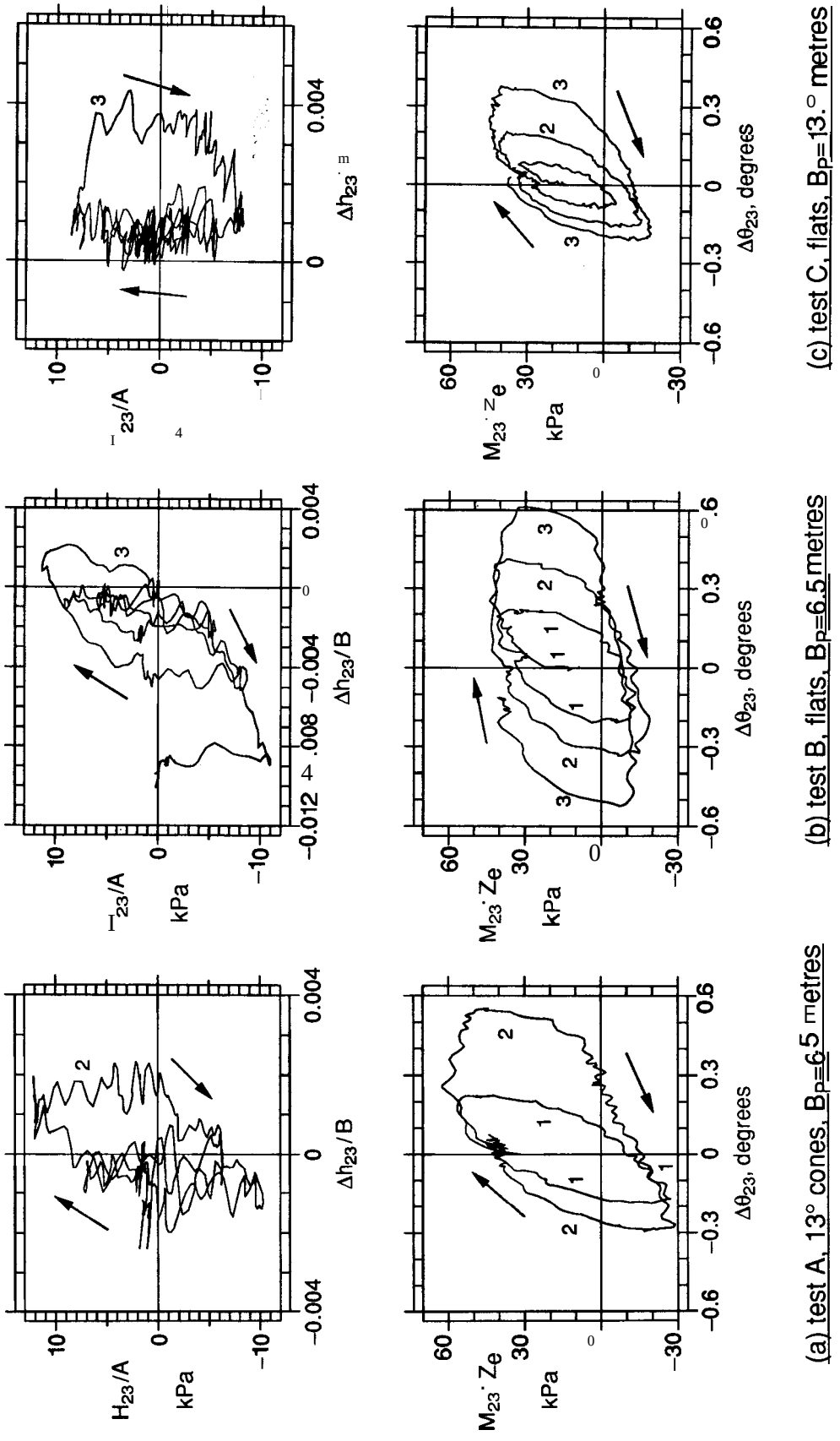

(a) test A, 13° cones, B_p=6.5 metres

(b) test B, flats, B_p=6.5 metres

(c) test C, flats, B_p=13.° metres

CUED 'D–Soils/ TR289	EVENTS N0.3. HORIZONTAL DISPLACEMENTS AND ROTATIONS AT THE SPUDCANS ON LEG 2 AND 3	FIG.NO. 12

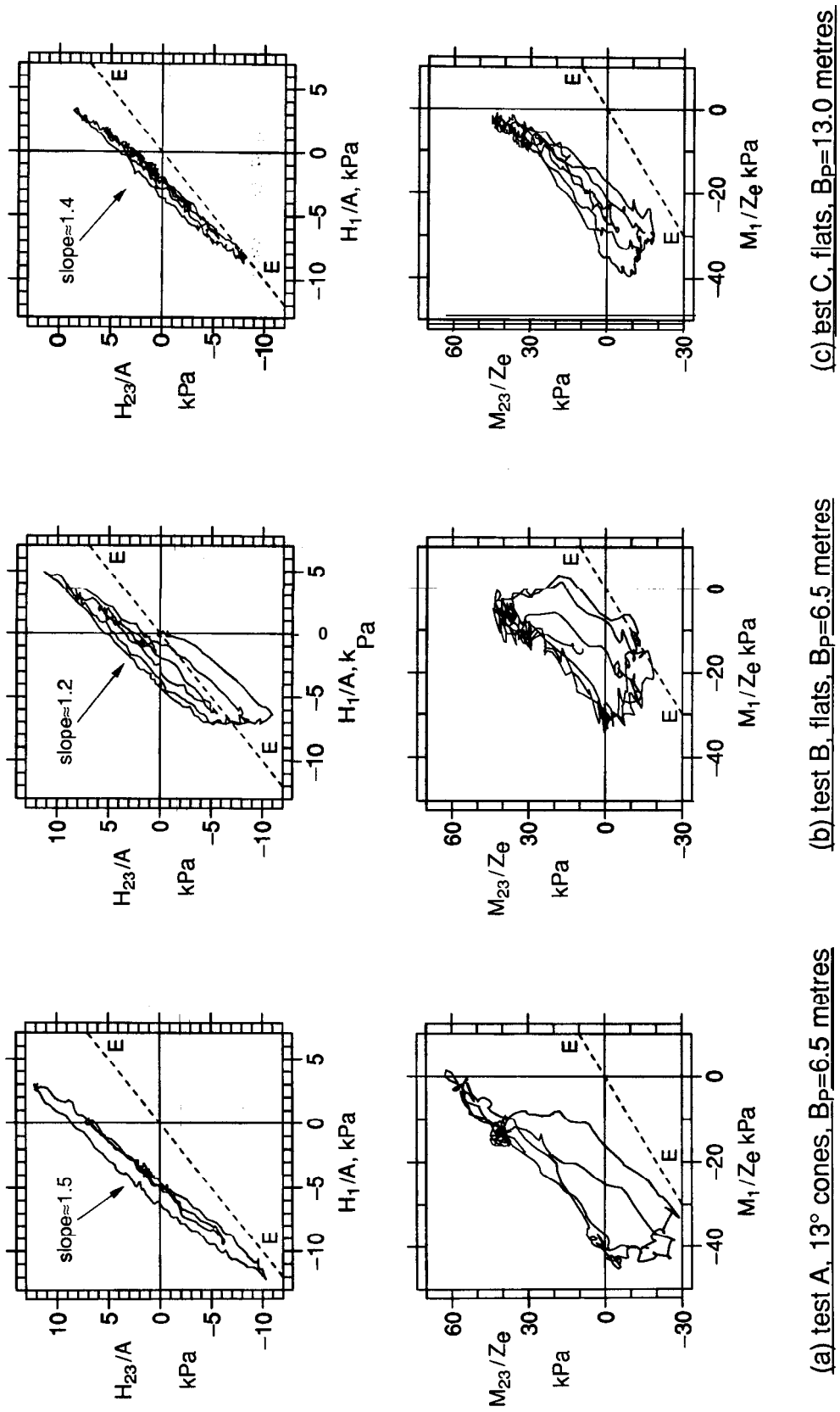

(a) test A, 13° cones, Bp=6.5 metres

(b) test B, flats, Bp=6.5 metres

(c) test C, flats, Bp=13.0 metres

CUED ID-Soils/ TR289	EVENTS N0.3. LOADSHARING BETWEEN SPUDCANS	FIG.NO. 13

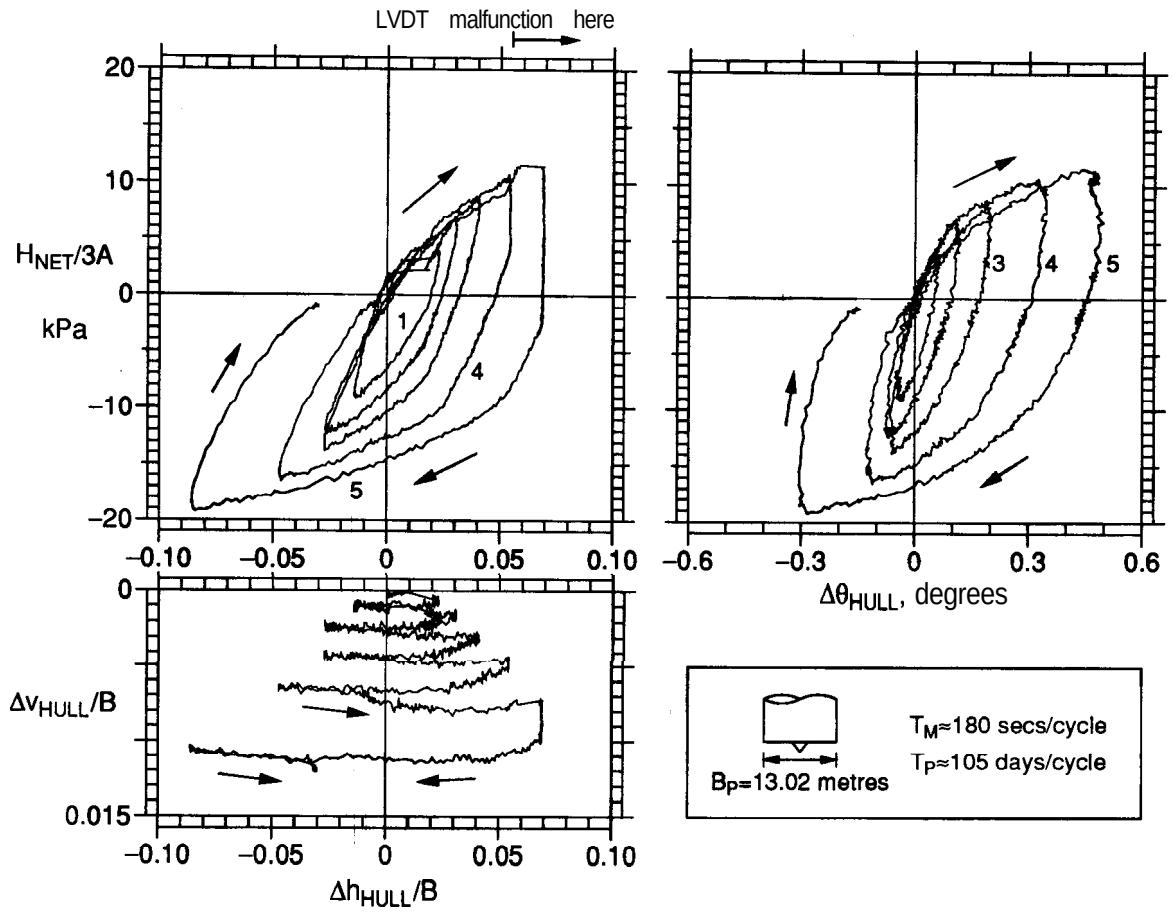

(a) hull responses

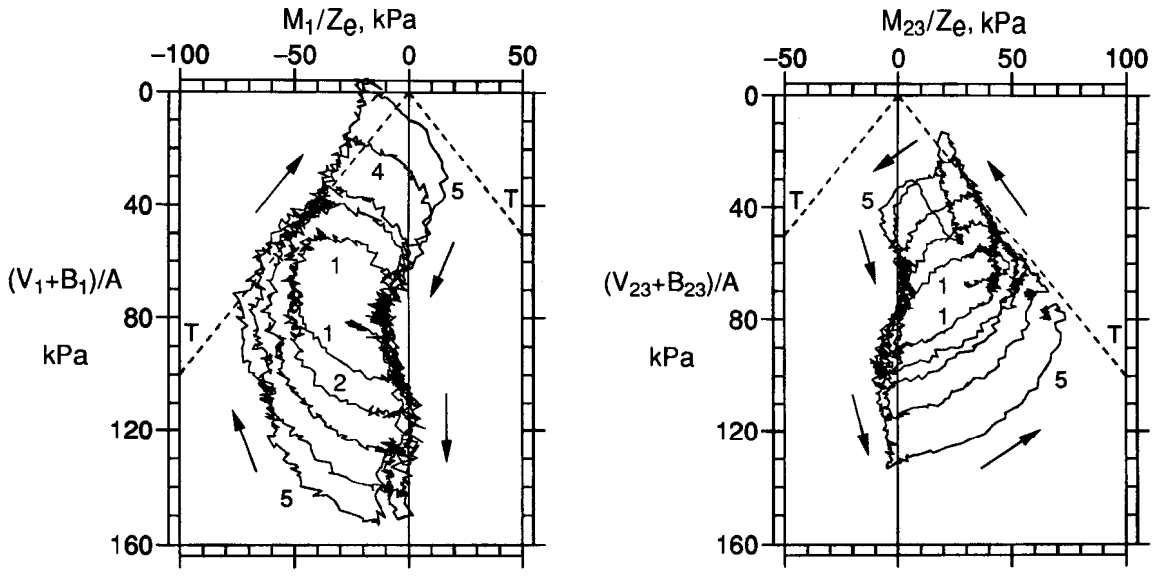

(b1) spudcan on lea 1

(b2) average at spudcans on leas 2 and 3

(b) soudcan moment-axial load resoonses

CUED 'D-Soils/ TR289	ASPECTS OF SLOW CYCLIC LOADING IN EVENT 9 OF TEST C	FIG.NO. 14

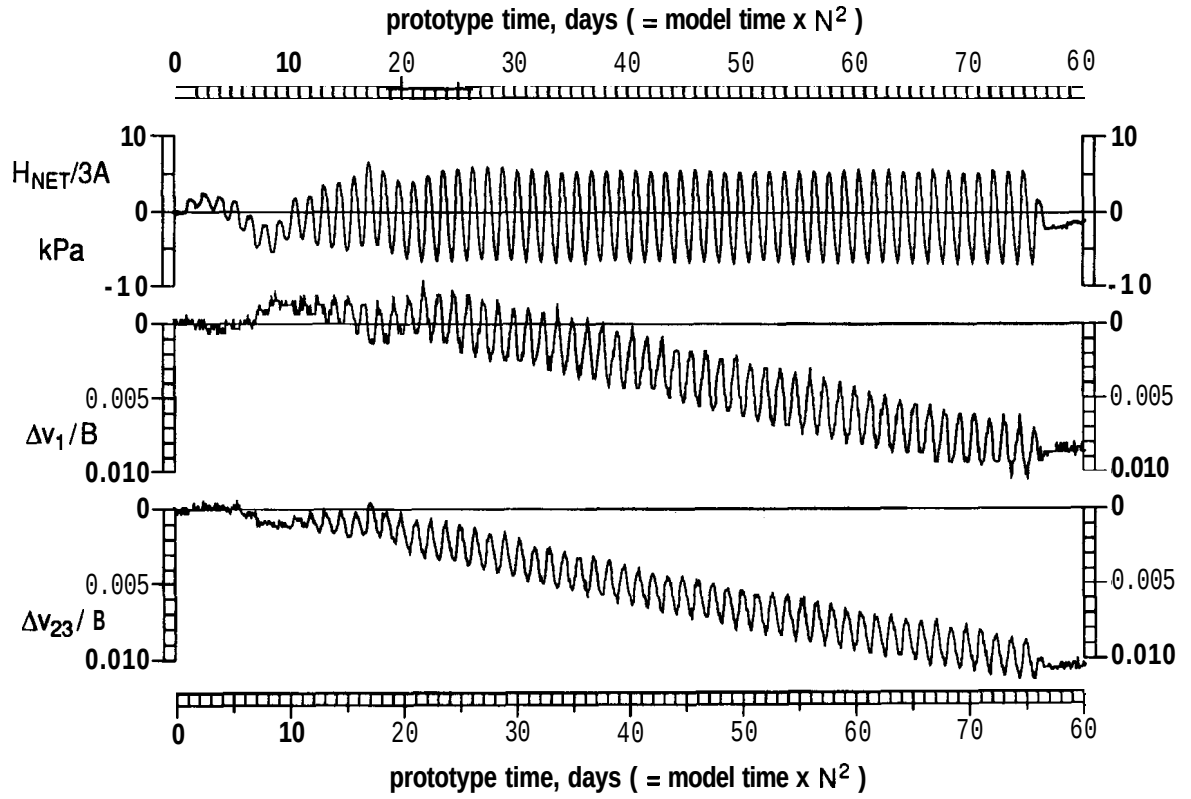

(a) time records of net horizontal load and spudcan settlements in event 8 of test B

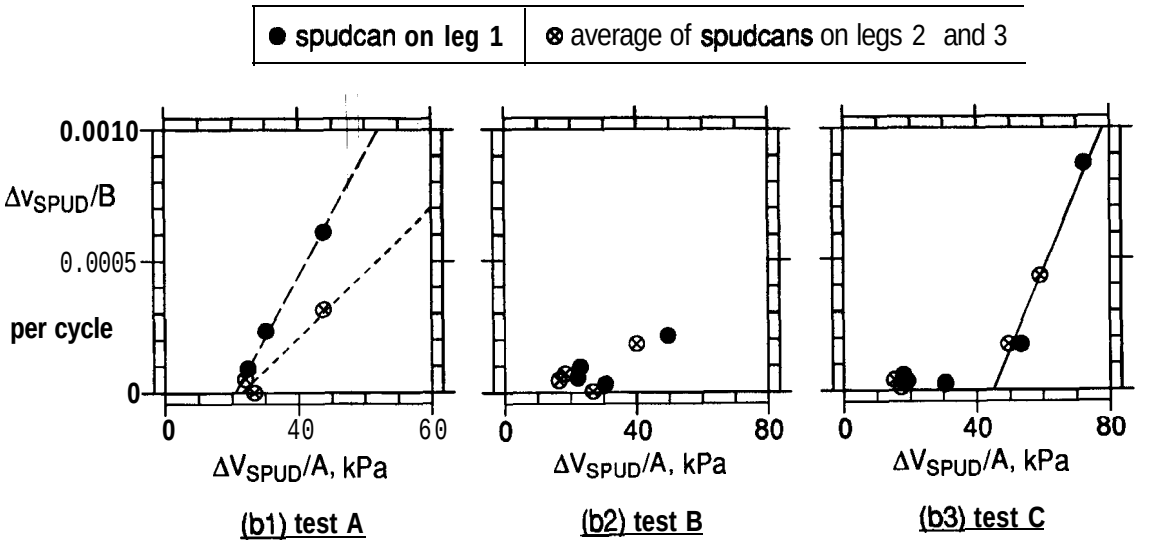

(b) net (plastic) vertical settlements per cycle

CUED /D-Soils/ TR289	SPUDCAN VERTICAL SETTLEMENTS DURING RAPID CYCLIC LOADING	FIG.NO. 15

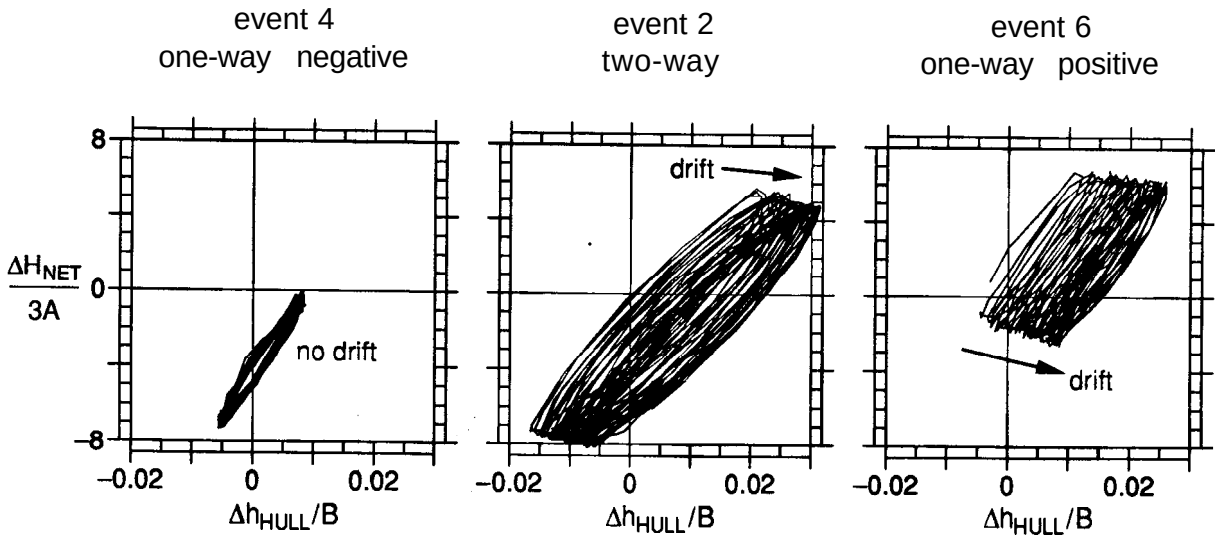

(a) hull horizontal load-displacement responses

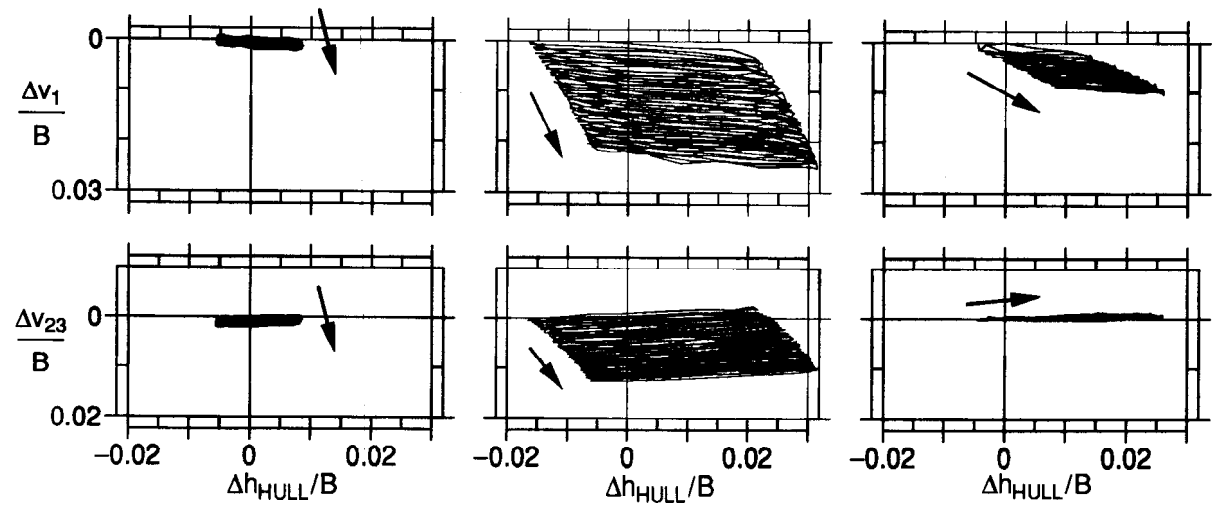

(b) spudcan vertical displacements

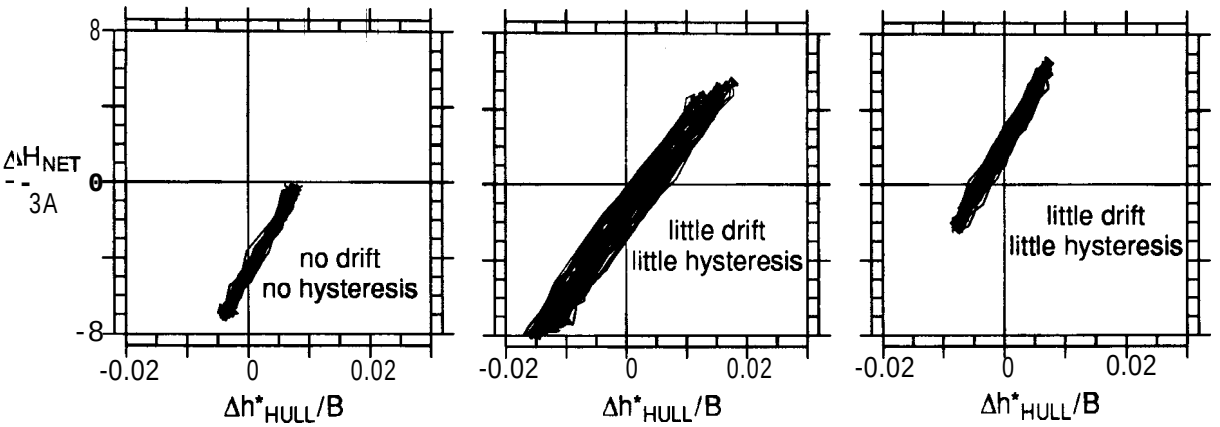

(c) hull horizontal responses with effect of differential spudcan settlements extracted

CUED /D-Soils/ TR289	ANALYSIS OF EFFECT OF MEAN HORIZONTAL LOAD AND DIFFERENTIAL SETTLEMENTS IN 34 CYCLES OF RAPID LOADING. TEST A, 13" CONES. G_{NOM}=128g, B_P=6.5 METRES, T_M≈8.8 SECS/CYCLE, T_P≈1.3 DAYS/CYCLE	FIG.NO. 16

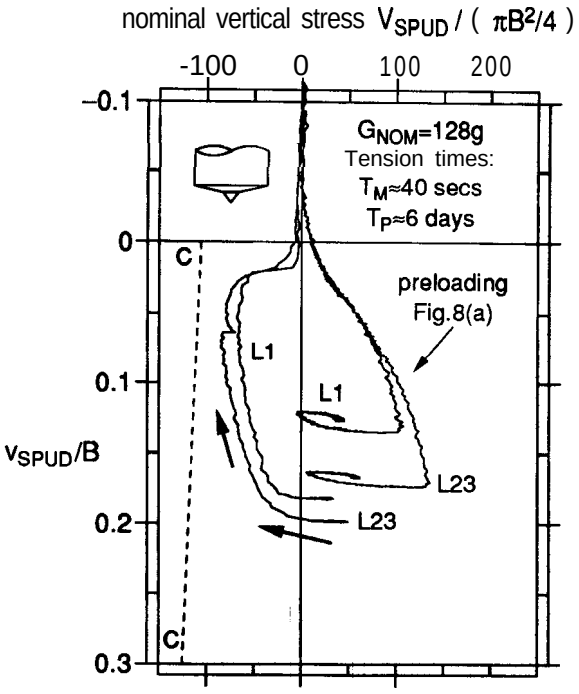

(a) test A. 13° cones, B_P=6.5 metres

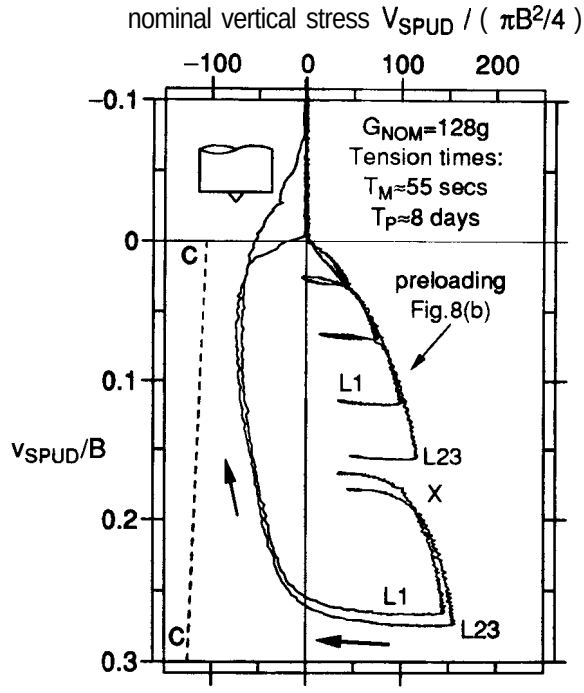

(b) test B, flats, B_P=6.5 metres

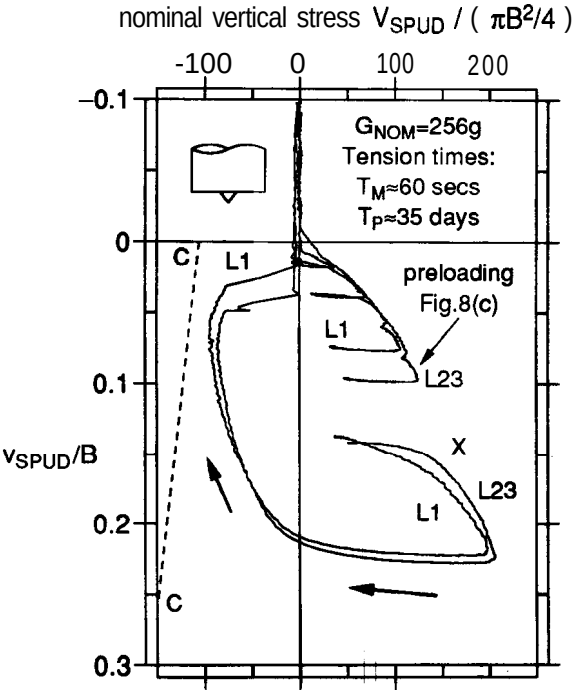

(c) test C, flats, B_P=13.0 metres

CUED 'D-Soils/ TR289	PRELOADING, VERTICAL RE-LOADING, AND PULLOUT DATA	FIG.NO. 17

Appendix 1. Notation

A	footing area at largest section, $= \pi B^2/4$
B	footing diameter at largest section (Bp=prototype diameter)
B_i	buoyancy upthrust on the spudcan on leg i
c_V, c_H	coefficient of consolidation, vertical, horizontal
D	distance between leg 1 and legs 2 and 3 in side elevation
e	voids ratio
EI	leg flexural rigidity
f	moment fixity, ratio of actual spudcan moment divided by theoretical value for a fully encastre foundation
g	acceleration of earth's gravity, $\approx$ 9.81 metres/sec^2
G_{NOM}	centrifugal acceleration at 1 metre radius from the drum axis
G_S	average specific gravity of soil particles
h	horizontal displacement
H_i	horizontal load on spudcan on leg i
H_{NET}	sum $H_1+H_2+H_3$ of spudcan horizontal loads
HLC	hull-leg connection
HRP	hull reference point
K_o	coefficient of lateral earth pressure
L	leg length, hull-leg connection (HLC) to spudcan-leg connection (SLC)
LRP	load reference point on spudcan
M	moment
N	scale factor
P	axial load
Q	shear load
r	radius from centrifuge axis
R	radius of centrifuge
R_{WS}	radius at model water surface
S	height of idealised rigid spudcan
SLC	spudcan-leg connection
T	time (T_M, T_P) or time factor ($T=c_V t/B^2$)
Q	shear load
U	upthrust applied to centrifuge model (Figure 5)
v	vertical displacement
V	specific volume, =1+e

V_i vertical load on spudcan on leg i equilibrated by the sum of soil effective stresses and excess pore pressure at the spudcan-soil interface.

$V_{i,total}$ total vertical load on spudcan on leg i, $=V_i+B_i$

w buoyant rig weight, $V_1+V_2+V_3$

W^* weight of model in centrifuge gravity (Figure 5)

Y height from spudcan LRP's to HRP, approx 352mm for the model here

z depth below soil surface

z_{MWS} depth below model water surface

Z_e footing equivalent elastic section modulus at largest section, $= \pi B^3/32$

A change of

$\Delta\theta_{DIFSET}$ jackup rotation due to differential spudcan settlement

$\Delta h_{HULL,DIFSET}$ hull horizontal displacement due to differential settlement

Δh^*_{HULL} hull horizontal movement adjusted to exclude effect of differential spudcan settlement (equation 11)

Γ,λ,κ constants in critical state model

θ rotation

ρ' buoyant mass density of soil, $=(G_S-1)./(1+e)$

ρ_W mass density of water, approximately 1000 kg/m^3

σ_V, σ'_V vertical total and effective stresses

σ'_θ circumferential effective stress

Subscripts

APP applied to the model (H_{APP} = horizontal load applied to model, Figure 5)

DIFSET due to spudcan differential settlement

H horizontal

HULL of the hull, at the hull load reference point

i quantity for the spudcan on leg i

M model (T_M = model time period)

MAX.PREV maximum previous value

NET total, net (H_{NET} = total horizontal load)

NOM nominal (G_{NOM}= centrifuge gravity at inner drum wall)

P prototype (B_P = prototype diameter, T_P=prototype time period)

SPUD quantity for a spudcan

V vertical

1 quantity for the spudcan on leg 1

23 average of quantities for the spudcans on legs 2 and 3